

Rotational and Near-IR Spectra of PbF: Characterization of the Coupled $X_1\ ^2\Pi_{1/2}$ and $X_2\ ^2\Pi_{3/2}$ States

Sean Jackson,^{*} Luke Kim,[†] Andreas Biekert,[‡] Alex Nguyen,[†] and Richard J Mawhorter[§]

*Department of Physics and Astronomy,
Pomona College, Claremont, CA 91711, USA*

Trevor J. Sears[¶]

Chemistry Department, Stony Brook University, Stony Brook, NY 11794-3400

Leonid V. Skripnikov, Vera V. Baturo, and Alexander N. Petrov^{**}

*Federal State Budgetary Institution “Petersburg Nuclear Physics Institute”,
Gatchina, Leningrad district 188300, Russia and
Saint Petersburg State University, St. Petersburg, 199034, Russia*

Jens-Uwe Grabow^{††}

*Gottfried Wilhelm Leibniz Universität,
Institut für Physikalische Chemie and Elektrochemie,
Hannover, 30167, Germany*

(Dated: September 6, 2024)

Abstract

Observations of the rotational spectrum of lead monofluoride, PbF, have been extended up to transitions in the $v = 7$ level for ^{208}PbF in the lowest $X_1\ ^2\Pi_{1/2}$ state of the radical and $v = 5$ for the ^{207}Pb and ^{206}Pb isotopologues. The data also include a few measurements for ^{204}PbF in $v = 0$. These new measurements have been combined with existing near-IR measurements of the $X_2 - X_1$ fine-structure transition and a simultaneous multi-isotope fit of the data to an effective isotope-independent ro-vibronic Hamiltonian has been carried out. The resulting parameters fully characterize the vibrational, rotational and hyperfine structure of the combined X_1 / X_2 state of the radical. A pair of opposite parity levels with total angular momentum quantum number, $F = 1/2$, in the lowest rotational level, $J = 1/2$ of ^{207}PbF are close in energy and their spacing decreases with vibrational excitation. The experimental results show the spacing decreases to less than 20 MHz at $v = 7$ and 8. The experimental work is complemented by new *ab initio* calculations which support the results and allow predictions outside the experimental data range. The calculated radiative lifetimes of the relevant vibrationally excited states are of the order of 50 ms. This work was motivated by interest in using ^{207}PbF as a vehicle for future probes of the standard model of physics such as placing limits on the electron's electric dipole moment (*eEDM*), molecular charge-parity non-conservation and Born-Oppenheimer breakdown effects for example.

I. INTRODUCTION

In 1978 the investigation of the electron's dipole moment (*eEDM*) and other parity non-conserving (PNC) effects in lead monofluoride, PbF, was suggested by Labzowsky and Gorshkov [1, 2] and Sushkov and Flambaum [3] who showed how these effects might be enhanced in diatomic radicals like BiS and PbF due to the closeness of levels of opposite parity in Ω -doublets having a $^2\Pi_{1/2}$ ground state. The first two-step *ab initio* calculation of PNC effects in PbF initiated by Labzowsky was completed by Titov et al. [4]. Much later, PbF emerged as a potential candidate molecule for experimental and theoretical studies of

* Graduated Pomona College, 2023

† Graduated Pomona College, 2018

‡ Graduated Pomona College, 2016

§ rjm04747@pomona.edu

¶ trevor.sears@stonybrook.edu

** alexandernp@gmail.com

†† jens-uwe.grabow@pci.uni-hannover.de

physics beyond the standard model when Shafer-Ray et al. [5] predicted that the electric field-dependent g -factor could cross zero at high electric fields.

This result suggested that the molecule could be an attractive target for experiments designed to place a limit on the size of the e EDM. In order to design such an experiment, knowledge of the detailed internal energy level structure of the molecule is necessary. In 2011, Mawhorter et al. [6] reported measurements of rotational transitions among the lowest rotational levels of the molecule that more fully characterized the ground state fine and hyperfine split energy level structure for all stable PbF isotopologues in natural abundance, ^{208}PbF (52.4 percent), ^{207}PbF (22.1 percent), ^{206}PbF (24.1 percent), and ^{204}PbF (1.4 percent). As just noted, due to the intrinsic orbital angular momentum in a $^2\Pi$ state, molecules containing even lead isotopes exhibit distinct Ω -doubling between opposite parity levels in the ground $X_1^2\Pi_{1/2}$ state with small ^{19}F nuclear hyperfine splittings. The handedness of this orbital angular momentum relative to the molecular axis provides inherent symmetry sensitivity akin to the handedness arising from the bending mode degeneracy in molecules like YbOH [7–10], but without the attendant polyatomic complications. For the even PbF isotopologues, opposite parity fine and hyperfine split rotational levels are well separated. In ^{207}PbF though, the large ^{207}Pb ($I_{\text{Pb}} = \frac{1}{2}$) hyperfine interaction causes a near cancellation of the Ω -doubling splitting in some levels resulting in a pair of levels of opposite parity only 266 MHz apart in the lowest rotational and vibrational level. Alpehi et al. [11] showed, on the basis of these results, how the ^{207}Pb -containing isotopologue was a particularly strong candidate for experiments designed to probe certain symmetry-breaking effects. Follow-up studies included a determination of centrifugal distortion parameters for the hyperfine structure constants [12] needed to refine hyperfine splitting calculations, and an investigation of the theoretical and experimental ^{208}PbF g -factors using Zeeman data [13].

In 2023 the JILA group obtained a new constraint on the e EDM, $|d_e| < 4.1 \times 10^{-30}$ $e\cdot\text{cm}$ (90% confidence) [14], using $^{180}\text{Hf}^{19}\text{F}^+$ ions trapped by a rotating electric field. This result can be compared with the latest ACME collaboration constraint obtained in 2018, $|d_e| < 1.1 \cdot 10^{-29}$ $e \cdot \text{cm}$ in a ThO beam experiment [15]. In both $^{180}\text{Hf}^{19}\text{F}^+$ and ThO the measurements were performed on the metastable excited electronic $^3\Delta_1$ states. The great progress in the e EDM search using these molecules is closely related to their Ω -doubling

structure. As was shown in Ref. [16] the Ω -doublet structure is arranged in such a way that e EDM contribution to the splitting is opposite to many systematic effects including the one related to stray magnetic fields. Thus, subtracting the measured energy splittings in the two Ω -doublet states suppresses many systematic effects in the experiment. Baturo et al. [17] showed the existence of a similar energy level structure for ^{207}PbF . Equally important, the small zero-field splitting between the opposite parity pair of levels in the lowest rotational level of ^{207}PbF actually decreases with increasing vibrational excitation, [18] reaching a minimum between $v = 7$ and 8 where the levels in question cross in energy.

The smaller the zero-field splitting between the opposite parity levels the smaller electric field required to polarize the molecule which reduces potential measurement systematics. Baturo et al. [17] also showed that while the g -factor in the lowest state of the molecule does not vanish, it is still very small thus reducing potential systematic errors in any future e EDM measurement due to stray magnetic fields. One can note that the set up of the experiment on trapped HfF^+ ions is very different from molecular beam experiments on ThO and (potentially) PbF . However, it is important to use different molecular systems to confirm the reliability of the measured e EDM limits. The main advantage of ^{207}PbF as compared to ThO is that the e EDM sensitive state of ^{207}PbF is in its ground electronic state. [Even the excited vibrational levels, where the parity spacing is minimized, have lifetimes that are far longer \(see Table IV below\) than the excited state lifetime of \$\text{ThO}\$ \(\$\sim 1\$ msec\). Level lifetimes directly translate to coherence times which linearly affect potential experimental sensitivity.](#)

^{207}PbF in its lowest X_1 state is also a good candidate for experiments designed to search for temporal variation in fundamental constants [19] as well as molecular level consequences of an anapole moment of the ^{207}Pb nucleus [11]. Recent work by Baturo et al. [17] has summarized the relevant spectroscopic work up to 2022. Since 2022, recent work by Luan et al. [20] investigated the suitability for laser cooling of the $X_2 - X_1$ near-IR electronic transition that is a focus of the present work. They showed that the highly diagonal nature of the band system made it possible to propose a four-laser scheme to reach submicro-Kelvin temperatures. Zhu et al. [21] recorded and analyzed a region of the $B^2\Sigma^+ - X_1^2\Pi_{1/2}$ band system in a jet-cooled sample of PbF . The analysis combined published near-IR data [22]

and microwave data [6] together with their new measurements, but was much less comprehensive and does not include the new data in the present work which also combines data for all the naturally occurring isotopes of the molecule.

Here, we report the measurement of many new hyperfine-split rotational transitions in all the naturally-occurring isotopic modifications of PbF. These new data include information on excited vibrational levels within the X_1 state that permit the experimental determination of the variation in energy of the parity and hyperfine-split levels in the lowest rotational level of ^{207}PbF with vibrational excitation. The data have been combined with existing and some newly assigned near-IR spectral data for the molecule, and a combined analysis determines the parameters appearing in the isotope-independent effective Hamiltonian describing the molecule. In the form of the Hamiltonian model used, the energies resulting from a Dunham-type expansion of parameters Y_{lm} , described in detail below, are fitted to the measured transitions. The spectroscopic analysis identified several Born-Oppenheimer breakdown contributions to the molecular energy levels. These include a non-zero isotopic variation in the equilibrium spin-orbit splitting, and field shifts due to finite-sized nucleus effects which cause systematic isotopic variation beyond the expected isotopic mass relationship in the rotational constant, among other parameters. These shifts have also been investigated theoretically. The results will be useful for predicting the energies of levels outside the set included in the present data, as well as the energies of other isotopologues, in particular ^{205}PbF where the odd lead nucleus with spin $I = \frac{5}{2}$ has a quadrupole moment and a half life of 17.3 million years.

The present work establishes the size of the splitting between the near-degenerate parity pair of ^{207}PbF levels, and its vibrational level dependence, to a precision and accuracy of a few kHz, as well as the energies of the rotational-vibration levels in the combined X_1 / X_2 fine-structure pair of levels in the ground $^2\Pi$ state of the molecule up to rotational quantum number, $N, \approx 60$ and vibrational levels, $v \leq 8$. The splitting between the near-degenerate parity pair with total angular momentum quantum number, $F, = 1/2$ in ^{207}PbF reaches a minimum of 15 MHz at $v = 8$. The experimental measurements are complemented by new *ab initio* calculations that compare well to the experimental results and permit extrapolation of the experimental data to still higher energy levels. In the spirit of the earlier work on the

g -factor variation with electric field [17], we have investigated the variation in the higher vibrational levels where the parity spacing is at its minimum. We also calculate the radiative lifetime for the $v = 8$ level of X_1 ^{207}PbF in question to be 38 ms, sufficient for future precision measurements that are not restricted by lifetime-limited experimental coherence times.

II. EXPERIMENTAL DETAILS

We have measured approximately 130 hyperfine-split rotational transitions among the lowest few rotational levels of the PbF radical in its ground, X_1 $^2\Pi_{1/2}$ state. The measured frequencies are given in the Appendix and together with the near-IR data included in the analysis, see section IV, are also available in a Pomona College thesis [23]. The data include transitions at frequencies between approximately 4 and 26 GHz covering the operating range of the spectrometer. While these are primarily between the lowest $J = 3/2$ and $1/2$ levels, the large Ω -doubling intervals of 4, 8, 12, and 16 GHz with increasing J enable access to the $J = 5/2$ and $7/2$ manifolds as well. The structure of the lowest few energy levels in the molecule is illustrated in Figure 1 of reference [6], which shows the profound influence of the spin $1/2$ ^{207}Pb nucleus. Here the near-degenerate ^{207}PbF parity pair are the levels labelled 3 and 4. This reference also includes a description of the form and effective parameters in the hyperfine Hamiltonian required to model the energy level structure.

The Fourier transform microwave (FTMW) spectrometer used has been described previously [24, 25] and PbF was synthesized *in situ* by laser vaporization of a sample of natural abundance Pb metal in the presence of a dilute sample of SF_6 entrained in neon gas prior to a supersonic free-jet. Frequencies were determined by the Fourier transform of the free induction decay from the resonator antenna. This enables sub-kHz resolution for transitions with good signal to noise.

Importantly, we have been able to improve the spectrometer's capability to record transitions in excited vibrational levels that, even after creation of a laser plasma, suffer from low population after collisional transfer during supersonic expansion. This has been compensated for by a direct current discharge[26] boosting the internal energy of the molecular

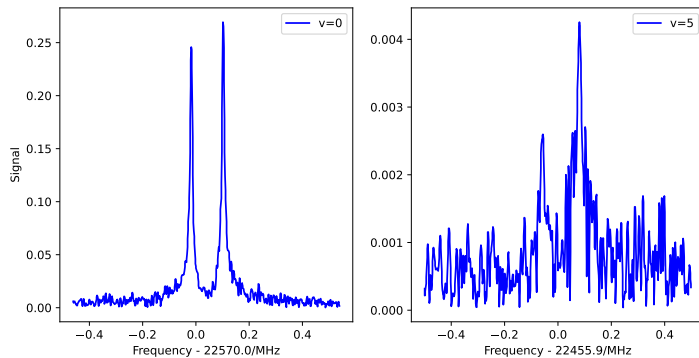


FIG. 1. Examples of FTMW transitions in $v = 0$ and 5 vibrational levels of ^{207}PbF . The resonance signal appears twice due to the Doppler shift of the expanding molecular jet’s emission with respect to the resonator mode’s propagation. The rest frequency is the arithmetic mean of the two frequencies. The experimental conditions were optimized for each transition.

sample prior to the expansion. This enabled a larger vibrational data set. There are potentially 20 $J = 3/2 \rightarrow 1/2$ observable transitions among the three most abundant PbF isotopologues. In vibrationally-excited levels 20, 15, 12, 9, and 6 were measured in the levels $v = 1-5$, respectively. Transitions in $v = 6$ and $v = 7$ were detected in the most abundant ^{208}PbF and a few transitions in the low-abundance variant, ^{204}PbF were also detected. The different mass isotopologues have predictably different transition frequencies and spectral assignments were usually straightforward. The requirement that all the different isotopic species data are consistent in the overall fitting provides strong limits against possible mis-assignments. Examples of the spectra involving $v = 0$ ground state and $v = 5$ excited vibrational levels of ^{207}PbF are shown in Figure 1.

III. THEORETICAL METHODS

To calculate potential energy curves and the dependence of the molecule-frame dipole moment on the internuclear distance, we employed the relativistic two-component coupled cluster method with single, double, and perturbative triple excitation amplitudes, known as CCSD(T) [27, 28]. In these correlation calculations, we excluded 60 inner-core electrons using the valence part of the relativistic effective core potential approach [29–31]. The basis set for Pb was constructed following the procedure outlined in Ref. [32] and consisted of 22

s-, 23 p-, 16 d-, 8 f-, 4 g-, and 3 h-type Gaussian functions. For F, we utilized Dyal’s uncontracted augmented all-electron quadruple-zeta basis set AAE4Z [33]. The results were also used to calculate lifetimes of excited vibrational states. To estimate the uncertainty of the lifetimes we compared results obtained at the CCSD(T) and at the coupled cluster singles and doubles, CCSD [27, 28] levels.

To calculate the dependence of the hyperfine structure parameters on the internuclear distance, we employed the 4-component relativistic CCSD(T) [28] approach within the Dirac-Coulomb Hamiltonian. For Pb, we utilized Dyal’s uncontracted AAE3Z [33] basis set, while for F, the AE3Z [33] basis set was used. In the correlation calculation, we excluded the $1s.3d$ electrons of Pb. The energy cutoff for virtual orbitals was set to 300 Hartree. Relativistic electronic structure calculations were performed using the DIRAC [34, 35] and MRCC [36–38] codes. The eigenvalues and eigenfunctions of the lead monofluoride molecule required for calculation of the sensitivities to variation of fundamental constants and to the e EDM were obtained by numerical diagonalization of the molecular Hamiltonian over the basis set of the electronic-rotational and nuclear spin wave functions. Details of the method can be found in Refs. [12, 13].

IV. DATA AND ANALYSIS

In order to characterize fully the mixed X_1/ X_2 $^2\Pi$ electronic state complex of PbF, we have combined the 130 measured microwave transition frequencies with the data published by Ziebarth et al. [22, 39] who measured spectroscopic emission transitions between the X_2 $^2\Pi_{3/2}$ and X_1 $^2\Pi_{1/2}$ fine structure states in the near-IR (NIR) region at $1.3 \mu m$. Figure 2 illustrates the vibronic transitions involved. Each of those shown in the figure includes many rotationally-resolved, and for ^{207}PbF hyperfine-resolved, transitions and there are data for the 3 most abundant naturally-occurring isotopic variants of the molecule. In addition to the transitions originally identified, [22, 39] we have assigned many transitions in the $v = (1,1)$ band in ^{208}PbF and ^{207}PbF . We are most grateful to Prof. E. Fink (Wuppertal) who generously provided us with a copy of the original data and additional details. The complete set of 1201 NIR and 130 FTMW spectroscopic transitions included in the present analysis is available in Jackson’s thesis [23].

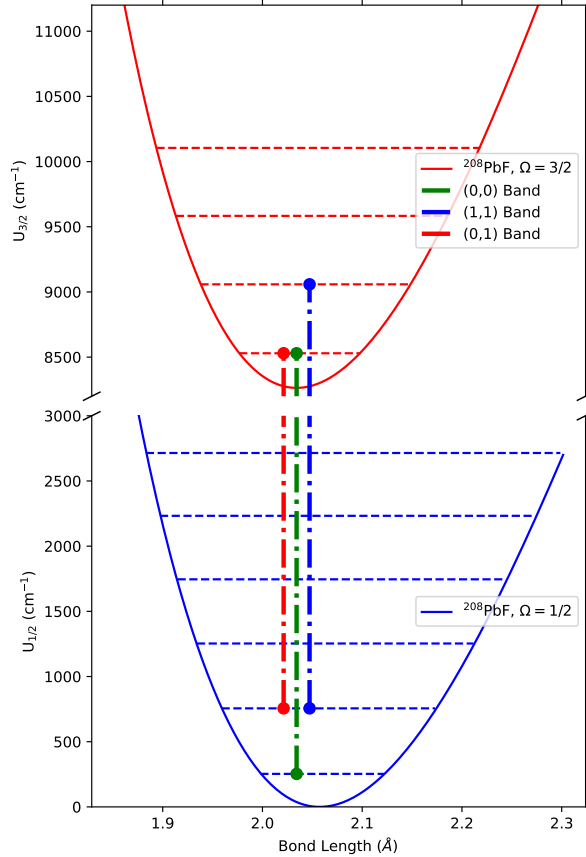


FIG. 2. Scheme of the fine structure transitions measured for ^{206}PbF , ^{207}PbF and ^{208}PbF . The potential curves and level positions are calculated from the present results

The analysis used the SPFIT code of the CALPGM package originally developed by Pickett [40, 41] for the purpose of categorizing astronomical line positions which has become a ubiquitous *de facto* standard in the field. Employing control code sequences, the elements comprising the Hamiltonian matrix are highly adaptable and can handle spectroscopic data of many types and precision, including multiple isotopic variants of a molecule in multiple vibrational levels with fine and nuclear hyperfine interactions. This allows the use of a Dunham-type expansion [42] to describe the molecular energy levels assuming standard reduced mass variation of the parameters. Details are given in the original description of the CALPGM suite of programs by Pickett [40] and a guide by Novick [41]. Dunham coefficients, $Y_{l,m}$, derived from fitting to experimental data can be related to parameters describing the diatomic potential function [43]. More details are given in the sections below.

A published analysis of data for the two bromine isotopes in BrO [44] illustrates many of the capabilities of the SPFIT package that are relevant to the present work. The form of the rotational energy terms, with the equilibrium rotational constant, B_e , Dunham coefficient Y_{01} , Λ -doubling parameter, p_{00} , and hyperfine parameters that were expressed in the Frosch and Foley representation [45] are discussed in detail by Brown and Carrington [46]. A brief overview is given below in section V B. Finally, small contributions from the nuclear spin-rotation coupling, C_I , for both ^{19}F and ^{207}Pb and the nuclear spin-spin dipolar coupling interaction, t_{00} , for ^{207}PbF , were found to be needed for the reproduction of the spectra at the accuracy and precision inherent to the FTMW data.

V. RESULTS AND DISCUSSION

A. Overall Fitting

The FTMW data give very precise information on rotational, Λ -doubling and hyperfine spacings in the X_1 component, but has little or no sensitivity to the larger fine-structure or vibrational spacings that define the position and properties of the upper X_2 component. On the other hand, the NIR data determine parameters describing the fine structure and vibrational spacings and also contain information on centrifugal distortion effects because the data extend to high rotational quantum number. Lower precision measurements for the upper X_2 component hyperfine and Λ -doubling splittings meant that some parameters involving them were not determinable. The spin-orbit splitting parameter A_e determines the spacing between the X_2 and X_1 states and is normally expected to be weakly vibrationally dependent and isotopically independent, however the data indicated these assumptions were invalid and the variation of the spin-orbit splitting was accounted for in a similar way to that adopted by Drouin et al. [44] in the case of BrO. More details are given in the following sub-sections. The numerical results are presented in Tables I, II and III.

B. Dunham Formulation

The global multi-isotope fit of the data to a Dunham-type expansion comprises 45 independent parameters, most of which describe the energy levels of a diatomic molecule within a series of products of powers of a vibrational quantum number-dependent term, $(v + 1/2)^l$,

TABLE I. Vibrational, fine-structure and rotational parameters derived from a global PbF fit of 1331 transitions (weighted fit $\sigma = 1.02$; see text). Parameters without parenthetical error values were kept at values calculated prior to the fit, see text for details. Isotopic scaling relations are from [44].

Parameter	^{208}PbF Molecular Parameters		Isotopic Scaling Relations
		Value ^a	Reduced Mass Ratio
Y_{10}		15593865.4(13)	$\mu^{-1/2}$
Y_{20} ^c		-66070(14)	μ^{-1}
Y_{01}		6937.14652(11)	μ^{-1}
Y_{01} (BOB)		-2.520(26) kHz	$\delta\langle r^2 \rangle$
V_{Pb} ^b	48.8(4)	(10^{-7} fm ⁻²)	none
Y_{11}		-44.10637(11)	$\mu^{-3/2}$
Y_{21}		0.080705(38)	μ^{-2}
Y_{31}		0.1713(37) kHz	$\mu^{-5/2}$
Y_{02}		-5.4844(72) kHz	μ^{-2}
A_e		247705376.9(46)	none
γ_{00}		-2513.6(44)	μ^{-1}
Y_{00}^*		5647.2	μ^{-1}
^{207}PbF ΔA_e^{iso}		199.2(21)	none
^{206}PbF ΔA_e^{iso}		312.0(22)	none
A_{10}		828312.4(56)	$\mu^{-1/2}$
A_{20} ^c		-23708(15)	μ^{-1}
A_{01}		156.9284(57)	μ^{-1}
A_{11}		1.0223(50)	$\mu^{-3/2}$
A_{02}		0.1804(13) kHz	μ^{-2}
p_{00}		-4142.46361(25)	μ^{-1}
p_{00} (BOB)		-5.240(63) kHz	$M_{ref} - M_\alpha$
$\Delta_{01}^{p_{00}}$ ^b	99.4(96)	(unitless)	none
p_{10}		-2.29053(25)	$\mu^{-3/2}$
p_{20}		0.238350(43)	μ^{-2}
p_{01}		-3.125(19) kHz	μ^{-2}

^a In MHz unless otherwise noted, 1σ deviation given in parenthesis.

^b The field shift, V_{Pb} , and the Born-Oppenheimer Breakdown (BOB) term, $\Delta_{01}^{p_{00}}$, were not determined from the fit directly. Fitted parameters that correspond to the offset values used in SPFIT program are Y_{01} BOB and p_{00} BOB. The quoted uncertainties for V_{Pb} and $\Delta_{01}^{p_{00}}$ were derived using the uncertainties of the fitted parameters and Equations 14 and 16.

^c Uncertainty in this parameter comes from a preliminary fit of the NIR data alone. The Y_{10} and Y_{20} parameters give the average of the harmonic and anharmonic vibrational constants between the X_1 and X_2 states. These parameters relate to Y_{lm}^* as in Equation 3. The $\omega_e x_e = Y_{20}^*$ values reported in [39] equal the Y_{20} (average) value here.

and a rotational term as $(N(N+1))^m$. Each operator term is preceded by a coefficient $X_{l,m}$, that is to be determined by a least squares minimization fitting the data. Parameter choices were guided by those used by Cohen et al. in their study [47] of isoelectronic BiO which included vibrational states up to $v = 9$.

TABLE II. ^{207}Pb hyperfine parameters derived from the global fit, as in Table I

Parameter	Value ^a	Reduced Mass Ratio
$a_{00(Pb)}$ ^b	2775(40)	g_N
$b_{F_{00}(Pb)}$	-2207(140)	g_N
$b_{F_{10}(Pb)}$	-27.4121(49)	$g_N\mu^{-1/2}$
$b_{F_{20}(Pb)}$ ^b	0.1257(17)	$g_N\mu^{-1}$
$c_{00(Pb)}$ ^b	-3584(200)	g_N
$d_{00(Pb)}$	7246.9964(22)	g_N
$d_{10(Pb)}$	34.0789(49)	$g_N\mu^{-1/2}$
$d_{20(Pb)}$	-28.6(19) kHz	$g_N\mu^{-1}$
$d_{01(Pb)}$	7.01(12) kHz	$g_N\mu^{-1}$
$C_{I_{00}(Pb)}$	0.07793(28)	$g_N\mu^{-1}$
$C_{I_{10}(Pb)}$	0.77(33) kHz	$g_N\mu^{-3/2}$
t_{00}	-3.41(78) kHz	g_N
Parameter ^c	Theory Value	Experimental Value
$A_{\parallel}(\frac{1}{2})$	9849, 9796 ^e	10146.6733(9) ^d
A_{\perp}	-6990, -6911 ^e	-7264.0287(25), -7264.0388(4) ^d
$A_{\parallel}(\frac{3}{2})$...	318(50)
$\tilde{A}_{\perp}(=b_{00(Pb)})$	-1012(120) ^b , -1217 ^e	...

^a In MHz unless otherwise noted, 1σ deviation given in parenthesis.

^b Determined iteratively from experiment ($a_{00(Pb)}$) and a combination of experiment and theory ($c_{00(Pb)}$).

$c_{00(Pb)}$ uses the $b_{00(Pb)}$ theoretical value. See Section V C for details, both were fixed in the final fit.

^c Alternative formulation of hyperfine terms. These parameters are not determined from the fit directly, rather they are calculated from the optimized Frosch-Foley a , b_F , c , and d parameters. The relationships are given in the text in Section V C.

^d Reference [6]

^e Reference [12]

To ensure the final parameters for the X_1/X_2 $^2\Pi$ electronic state complex also reproduce vibronic level spacings to higher vibrational quantum number derived from lower resolution spectra reported by Lumley and Barrow [48, 49] and the initial Ziebarth et al. [39] data, a preliminary fit of all the NIR data including the vibronic spacings from Ref. [39] to determine the harmonic and anharmonic vibrational constants Y_{10} and Y_{20} and their corresponding A_{lm} corrections was performed. The global fit including the FTMW data was then performed with Y_{20} fixed and the two steps repeated to ensure convergence. Below, we summarize some of the essential attributes of the Dunham expansion model as implemented here.

TABLE III. ^{19}F hyperfine parameters derived from the global fit, as in Table I

Parameter	Value ^a	Reduced Mass Ratio
$a_{00(F)}$	129(5)	g_N
$b_{F_{00(F)}}$	49.2418(12)	g_N
$b_{F_{10(F)}}$	3.0314(13)	$g_N\mu^{-1/2}$
$b_{F_{20(F)}}$	-21.09(26) kHz	$g_N\mu^{-1}$
$c_{00(F)}$	-308(17)	g_N
$d_{00(F)}$	-255.03763(58)	g_N
$d_{10(F)}$	-1.91608(71)	$g_N\mu^{-1/2}$
$d_{20(F)}$	20.35(16) kHz	$g_N\mu^{-1}$
$d_{01(F)}$	-0.536(66) kHz	$g_N\mu^{-1}$
$C_{I_{00(F)}}$	4.401(79) kHz	$g_N\mu^{-1}$
Parameter ^b	Theory Value ^b	Experimental Value ^b
$A_{\parallel}(\frac{1}{2})$	412(11)	409.8416(14)
A_{\perp}	254(2)	255.9906(7)
$A_{\parallel}(\frac{3}{2})$	34.3(21)	...
$\tilde{A}_{\perp}(=b_{00(F)})$	153.0(92)	...

^a In MHz unless otherwise noted, 1σ deviation given in parenthesis.

^b These parameters are not determined from the fit directly, rather they are calculated from the optimized Frosch-Foley a , b_F , c , and d parameters. The relationships are given in the text in Section V C.

The rotational and vibrational energy levels can be calculated as described in [43]:

$$\frac{E_{vN}}{h} = \sum_{l,m} Y_{l,m} (v + \frac{1}{2})^l N^m (N + 1)^m \quad (1)$$

Here, the Y_{lm} are the Dunham coefficients and we have adopted the case (b) [46] definition of the rotational angular momentum, $\mathbf{N} = \mathbf{J} - \mathbf{S}$, as used in the SPFIT code. The first few terms in the rotation-vibration energy, for example, are given by

$$\begin{aligned} \frac{E_{vN}}{h} = & Y_{10}(v + \frac{1}{2}) + Y_{20}(v + \frac{1}{2})^2 + Y_{01}N(N + 1) + Y_{11}(v + \frac{1}{2})N(N + 1) + \\ & Y_{21}(v + \frac{1}{2})^2N(N + 1) + Y_{31}(v + \frac{1}{2})^3N(N + 1) + Y_{02}N^2(N + 1)^2 + Y_{03}N^3(N + 1)^3 \end{aligned} \quad (2)$$

Additional terms may be added as needed to adequately fit the data. Other angular momentum operator-based terms representing Λ -doubling and nuclear spin hyperfine interactions were added in a similar fashion [44].

A complication in PbF comes from the fact that the X_1 and X_2 fine structure components in the molecule have different potentials and therefore exhibit different effective vibrational frequencies. This difference is handled by defining a modified set of Dunham coefficients (Y_{lm}^*) for each fine-structure component:

$$Y_{lm}^* = Y_{lm} \pm A_{lm}/2. \quad (3)$$

where Y_{lm} are the standard Dunham coefficients, Eqns. (1,2), that may be thought of as representing the average potential and the upper and lower signs in (3) refer to the X_2 and X_1 component respectively. The A_{lm} are the fine structure energy contributions derived from the coefficient of the base operator term $A_e L_z S_z$ in the Hamiltonian, defined analogously to the Y_{lm} :

$$A_v = A_{00} + A_{10}(v + \frac{1}{2}) + A_{20}(v + \frac{1}{2})^2 + \dots \quad (4)$$

and, to account for additional non Born-Oppenheimer subtleties discussed below and in section V E:

$$A_{00}^{iso} = A_e + (Y_{00}^*({}^2\Pi_{3/2}) - Y_{00}^*({}^2\Pi_{1/2})) + \Delta A_e^{iso}, \quad (5)$$

for the lower X_1 and upper X_2 component vibrational frequencies and anharmonicities in cm^{-1} units. Note that the various spin-orbit A parameters appearing in the equations above include ΔA_e^{iso} , an additional isotopic variation not normally encountered, due here to a Born-Oppenheimer breakdown effect due to the variation in Pb-nuclear size. More discussion of this effect is included in section V E. We find $\omega_e(X_1, X_2) = (506.341(1), 533.970(1)) \text{ cm}^{-1}$ and $\omega_e x_e(X_1, X_2) = (2.599(1), 1.809(1)) \text{ cm}^{-1}$, in reasonable agreement with earlier band head measurements in [49], [50] and [39], as well as recent calculations [20], taking into account the differences in experimental resolution and basis set dependence, respectively.

To obtain the experimental fine structure spacing we need to add $-\gamma$ to agree with the numbers in reference [6], see subsection V D. The difference between the upper and lower component potentials is obvious in Figure 2 where the potential curves were computed using potential parameters derived from the final Dunham expansion parameters in Table I and the relationship between the Dunham coefficients and potential coefficients [43].

In the limit where the Born-Oppenheimer approximation holds, the constant A_e is isotope-independent[44], but this was not found here for PbF. The parameters in (5), $Y_{00}^* = (Y_{00}^*(^2\Pi_{3/2}) - Y_{00}^*(^2\Pi_{1/2}))$ and ΔA_e^{iso} account for the observed deviations. The Y_{00}^* parameter is a correction term describing the difference between A_{00} and A_e , or the difference between the (experimentally measured) fine structure interval for the $v = 0$ levels and the equilibrium fine structure spacing of the X_2 and X_1 $^2\Pi$ components. In the multi-isotope fit, A_e is for the reference ^{208}Pb isotope. The Y_{00}^* parameters for ^{207}PbF and ^{206}PbF are isotopically scaled from the ^{208}PbF Y_{00}^* value by μ^{-1} [44]. While these terms should account for the isotopic dependence of A_{00} leading to a constant A_e , as is the case for BrO [44] there remained (small) systematic deviations between the A_e spacing in the different isotopologues and these deviations are the ΔA_e^{iso} parameters in the results. No isotopic scaling relation is assumed for the ΔA_e^{iso} values; they are simply constant correction terms of the order of .0001% of the value of A_e corresponding to the ≈ 100 MHz nonlinearity in the isotopic dependence of A already observed by Ziebarth et al. [22]. In subsection VE, they are interpreted as energy contributions due to finite-sized nucleus effects.

The Dunham formulated parameters relate to conventional rotational and centrifugal distortions parameters as

$$B_v = Y_{01} + Y_{11}(v + \frac{1}{2}) + Y_{21}(v + \frac{1}{2})^2 + Y_{31}(v + \frac{1}{2})^3 + \dots \quad (6)$$

for the effective rotational constant, and

$$D_e = -Y_{02} \quad (7)$$

and

$$H_e = Y_{03} \quad (8)$$

for the centrifugal distortion constants.

C. Hyperfine Parameters

For a ${}^2\Pi$ molecule like PbF, Frosch and Foley [45] showed there are, in principle, four hyperfine coupling terms that need to be specified for each nuclear magnetic moment in the molecule. The terms in the effective Hamiltonian have coefficients conventionally labeled a , b , c and d . The first represents the coupling between the electronic orbital angular momentum projection, Λ , and the nuclear spin angular momentum, while the remaining three terms can be cast as combinations of the zero and second rank spherical tensor operators representing the coupling between the unpaired electron spin and the nuclear spin angular momenta. Brown and Carrington [46] detail the operator forms and show how they are related to classical dipole-dipole coupling terms.

From the electron spin resonance (ESR) literature the tensor nomenclature $A_{\parallel}(1/2)$, $A_{\parallel}(3/2)$, A_{\perp} and \tilde{A}_{\perp} has also been utilized [6, 12]. The parallel quantities represent linear combinations of Frosch and Foley terms entering in the diagonal matrix elements for the $X_1 {}^2\Pi_{1/2}$ and $X_2 {}^2\Pi_{3/2}$ wave-functions and are related to the Frosch and Foley coefficients by $A_{\parallel}(1/2) = (2a - b - c)$ and $A_{\parallel}(3/2) = (2a + b + c)/3$. Note that Brown and Carrington introduce the analogous quantities $h_{1/2} = A_{\parallel}(1/2)/2$ and $h_{3/2} = 3A_{\parallel}(3/2)/2$. The physically important Fermi Contact interaction is $b_F = b + c/3$, while the angular dependence of the electron-nuclear spin dipolar interaction is contained in the constants c and d . The latter is equal to $-A_{\perp}$ and determines the parity variation in the coupling of the spin dipole-dipole coupling while the constant c is related to the the Y_{20} spherical harmonic distribution of the electronic wavefunction [46]. Finally, $\tilde{A}_{\perp} = b$.

The FTMW data determine the combinations $(2a - (b + c))$, i.e. $A_{\parallel}(1/2)$, and d , i.e. $-A_{\perp}$ for the ${}^{207}\text{Pb}$ nucleus in ${}^{207}\text{PbF}$. When the ${}^{207}\text{PbF}$ $X_2 - X_1$ NIR data were included in the analysis some additional flexibility in the model was found to be needed in order to model the data to the measurement precision and accuracy. After some trials, we combined information from theory to pin the value of $\tilde{A}_{\perp}(= b)$ and optimized the Frosch and Foley a parameter to the observed ${}^{207}\text{PbF}$ NIR data while forcing the combination of parameters $A_{\parallel}(1/2)$ at the value of 10146.7 MHz obtained previously [6, 12] from the FTMW $v = 0$ data. The complete dataset was then fit to determine a corresponding value for b_F as well

as d . Note that $d = -A_{\perp}$ is functionally independent of the other hyperfine parameters since it only determines the difference in hyperfine splittings between levels of opposite parity. These steps were repeated until convergence. In this way, we obtain estimates for all the Frosch and Foley parameters which are given, with their statistical uncertainties, in Table II. A similar procedure was used to determine the analogous ^{19}F hyperfine parameters given in Table III.

D. Separating A_{01} and γ_{00}

A_{01} , the centrifugal correction to the spin-orbit coupling and γ_{00} , the electron spin-rotation coupling, appearing as $\gamma_{00}(\mathbf{N} \cdot \mathbf{S})$ in the Hamiltonian, have indistinguishable effects on the energies [50]. The physical interactions described by these parameters are distinct, but their contributions to the energy levels of the molecule are not, which makes them difficult to determine separately using spectroscopic data. Brown and Watson [50] showed that A_{01} , or A_D in their notation, and γ_{00} may be separated by using data from multiple isotopic variants of the molecule and individually determined from the equation:

$$\frac{\tilde{A}_{01}}{Y_{01}} = \frac{A_{01}}{Y_{01}} - \left[\frac{2Y_{01}}{A_e - 2Y_{01}} \right] \left(\frac{\gamma_{00}}{Y_{01}} \right). \quad (9)$$

Here, \tilde{A}_{01} is the effective A_{01} parameter determined when γ_{00} is held at zero in a fit to spectroscopic data for a single isotopic variant of a molecule. The actual A_{01}/Y_{01} and γ_{00}/Y_{01} ratios are isotope independent; they have identical isotopic mass ratios. The true values of A_{01} and γ_{00} can therefore be determined by using data for multiple isotopes to form simultaneous equations (9) and solving them for the constants.

γ_{00} enters linearly in the energy expression for the X_1 component [46] and it is therefore also very strongly correlated with A_e . Within the experimental measurement precision, the FTMW data are not sensitive to A_e at all, so only the NIR transitions were used in a procedure to separate the spin-rotation and centrifugal distortion to the spin-orbit coupling. An initial value for γ_{00} was estimated from second-order perturbation theory. Here $\gamma_{00} = (A_{00}^{iso} \times Y_{01})/\Delta E$ assuming a model where only a single $^2\Sigma^+$ state of PbF [51] at an excitation energy of $22\,500\text{ cm}^{-1}$ contaminates the lowest X_1 component of the ground $^2\Pi$ state [46].

Then, we estimate that the second-order contribution to γ_{00} is

$$\gamma_{00}^{(2)} = -\frac{A_e \times Y_{01}}{2.25 \times 10^4} \approx -0.078 \text{ cm}^{-1} \text{ or } -2300 \text{ MHz.} \quad (10)$$

The NIR data for all isotopes of PbF were then fit together assuming A_{01} and γ_{00} obey their known isotopic mass ratio dependencies, as in Table I, thus forcing the ratios of A_{01}/Y_{01} and γ_{00}/Y_{01} to remain constant for each isotopologue. In this way, we enforce the relationship between the two parameters in equation (9), and determine both a γ parameter and an A_{01} parameter simultaneously. The value for A_e was adjusted iteratively to match the fine structure splitting until convergence. The final value determined for γ_{00} of -2513.6(44) MHz (see Table I) is close to that estimated from equation (10).

Due to the indistinguishable nature of A_{01} and γ_{00} previous analyses have not utilized a γ parameter. Including the nonzero γ_{00} affects the $X_2 - X_1$ spin-orbit splitting as it enters linearly in the X_1 energy. With γ_{00} included, we find values of 248 116 740, 248 117 020, and 248 117 216 MHz for the splitting in ^{208}PbF , ^{207}PbF and ^{206}PbF respectively, in excellent agreement with the multiple values in [6].

The final parameters reproduce the observed spectroscopic data to within the measurement uncertainty. The overall standard deviation of the multi-isotope fit was 1.02 relative to the measurement uncertainties, reflecting a very satisfactory result. The resulting parameters may be used to predict the positions of unobserved levels and, in particular, to estimate the splitting between the low-lying, opposite parity levels of interest in ^{207}PbF . These spacings were not measured directly but the derived parameters from our analysis permits their estimation. The results are given in column 5 of Table IV, where they are also compared to the computed spacings based on the *ab initio* results. The experimental results show that the spacing is a minimum of 15.1 MHz with an uncertainty of less than 100 kHz, in the excited vibrational level, $v = 8$.

TABLE IV. Vibrational energies, lifetimes in the $X_1 \ ^2\Pi_{1/2}$ state of ^{208}PbF and the $J=(\frac{1}{2})^+$, $F = \frac{1}{2}$, and $J=(\frac{1}{2})^-$, $F = \frac{1}{2}$ parity level splitting in ^{207}PbF .

Vibrational Level, v	Experimental ^a cm ⁻¹	Calculated ^b cm ⁻¹	Lifetime ^b msec	\pm Parity State Experiment ^a	Spacing / MHz Calculated ^b
0	0.0	0.0	^c	266.285(2)	266.3
1	502.72	502.2	277(28)	233.505(5)	232.8
2	1000.89	999.8	141(15)	200.037(9)	199.3
3	1494.49	1492.9	95(10)	165.881(15)	164.9
4	1983.54	1981.5	72(7)	131.039(24)	129.9
5	2468.02	2465.6	59(6)	95.513(34)	94.0
6	2947.94	2945.3	49(5)	59.304(47)	57.4
7	3423.31	3420.7	43(4)	22.415(61)	20.4
8	3894.11	3891.6	38(4)	-15.152(78)	-17.1
9	4360.36	4358.3	34(3)	-53.394(97)	-47.4

from Tables I, II and III. Where shown, one standard deviation uncertainty is given in parenthesis in units of the last quoted decimal place. .

^a Calculated using the fit parameters and their associated errors

^b CCSD(T) method. Computational details are given in Section III

^c This is the lowest vibronic level.

E. Field Shifts and Born-Oppenheimer Breakdown Effects

Molecular field shift effects were first observed in the seminal 1982 studies of related lead chalcogenide and thallium halide diatomics [52, 53]. Based on ideas developed to explain field shifts in atomic spectra, Schlembach and Tiemann [52] showed how changes in the Coulomb potential experienced by the electrons in a molecule due to the finite size of nuclei can be accounted for. The imposition of isotopic mass-scaling relationships between the Y_{lm} in the present analysis resulted in small (few kHz) systematic errors in the fit residuals due to the different isotopic field shifts. Deviations of this type from conventional spectroscopic models are known as Born-Oppenheimer breakdown (BOB) effects and are one manifestation of a larger set of consequences of the Born-Oppenheimer separation of electronic and nuclear motion [54] that is implicitly assumed in the use of a Dunham expansion to describe the molecular energies.

More recent theoretical studies of field shift effects on rotational [55] and vibrational [56] spectra for PbTe, TlI, PtSi and the original PbX and TlX molecules, respectively, give summaries of the topic and also present new relativistic calculations. Almoukhalalati et

al. [56] also include the 2007 study of PbO [57] in their analysis. Knecht and Saue [55] pointed out a factor of π^2 (≈ 10) inconsistency in a 1985 follow-up study by the Tiemann group [58] which Prof. Tiemann has recently confirmed [59]. Hence their field shift quantities quoted below are from the original 1982 study by Schlembach and Tiemann. Other examples have been noted in our recent work on AlCl, BiF, and BiCl [60] as well as BaF [61].

In fact, we need to allow for these effects in not only the rotational constants, Y_{01} , but also in the parameters for Λ -doubling, p_{00} , and the spin-orbit coupling, A_e (as noted in subsection VB) as described by Watson [54] and Brown and Carrington [46]. Fluorine has only one stable isotope, so for PbF the Y_{01} BOB term on isotopic substitution of nucleus X' for reference nucleus X is given in the Schlembach-modified Watson model by [57]

$$Y_{01} = \mu^{-1}\bar{U}_{01} \left[1 + m_e \frac{\Delta_{01}^X}{M_{X'}} + V_X \delta \langle r^2 \rangle_{XX'} \right] \quad (11)$$

where μ is the reduced mass, m_e is the electron mass, $M_{X'}$ is the atomic mass of the substituted isotope, Δ_{01} is a Watson-type mass-dependent BOB correction and $V_X \delta \langle r^2 \rangle_{XX'}$ is the field shift term that depends on the change in mean square charge radii between the two nuclei X and X' . The \bar{U}_{01} term is:

$$\bar{U}_{01} = U_{01} (1 + V_X \langle r^2 \rangle_X) \quad (12)$$

where U_{01} is the isotope-independent rotational spectral parameter, $U_{01} = \mu Y_{01}$, and the $\langle r^2 \rangle$ term is the mean square charge radius of the reference nucleus X . Further discussion of mean square radii changes and a table of values for $\delta \langle r^2 \rangle$ are given in [62].

In the fitting, these correction terms were implemented as additive corrections to the isotopically scaled Y_{01} parameter for each isotopologue, Y_{01}^α . ^{208}PbF is the reference isotopologue, and field shift corrections were added to the isotopically scaled values of Y_{01} for the other three isotopologues. We can then calculate the value of the field-shift correction term V_{Pb} as

$$Y_{01}^\alpha + (FSC) = \mu_\alpha^{-1} \bar{U}_{01} [1 + V_{Pb} \delta \langle r^2 \rangle_{Pb, Pb'}], \quad (13)$$

where the FSC term is the required field shift correction determined from the fitting, and

the α index denotes different isotopologues of PbF. This equation can be rearranged for V_{Pb} as

$$V_{Pb} = \left(\frac{Y_{01}^\alpha + (FSC)}{\mu_\alpha^{-1} \bar{U}_{01}} - 1 \right) / \delta \langle r^2 \rangle_{Pb, Pb'} . \quad (14)$$

Using the values determined for the field shift correction, Y_{01}^α , and \bar{U}_{01} , we find $V_{Pb} = 48.8(4) \times 10^{-7} \text{ fm}^{-2}$.

For most high-Z atoms like Pb and Tl discussed here, the heaviest isotope is the most abundant. This generally determines the reference isotopologue, as is the case here with ^{208}PbF . Hence successive isotopologues in equation (11) move from heaviest to lightest and both the Δ_{01}^X and V_X terms are consistent with experimentally observed negative Y_{01} offsets. This is the case because (1): Δ_{01}^X is negative and the lighter isotope masses in the denominator of the mass-dependent term make this term more negative in an essentially linear fashion, and (2): although V_X is positive, progression to lighter nuclei generally leads to an increasingly negative trend in $\delta \langle r^2 \rangle$ and thus in the overall nuclear size dependent field shift term as well.

The difference between the Δ_{01}^X and V_X terms is that the individual $\delta \langle r^2 \rangle$ values lend physically significant shape to the V_X negative trend. This helps explain the generally better fits in the literature to the residuals using only the field shift term (i.e. $\Delta_{01}^X \equiv 0$) than when using only the more rigid linear mass-dependent term (i.e. $V_X \equiv 0$). Of course this is particularly true when the field shift term is much larger than the mass dependent term, which we expect to be the case for PbF. Indeed, Figure 3 shows that the residuals follow the shape and trend of the $\delta \langle r^2 \rangle$ values almost exactly. Numerically, a one parameter V_X fit has an RMS of 1.0197, very close to the minimum RMS of 1.0195 with all 4 residuals floating independently. In contrast, for a rigidly linear one parameter mass-dependent fit this quantity grows significantly worse to 1.0421.

As noted by previous authors, the resulting very strong correlation between these terms in many cases precludes cleanly untangling them. In some cases, e.g BaF [61], a strong odd-even variation in $\delta \langle r^2 \rangle$ can help significantly, but that is not the case for Pb or Tl (which has only 2 stable isotopes). The Δ_{01}^X term itself is made up of three smaller Dunham,

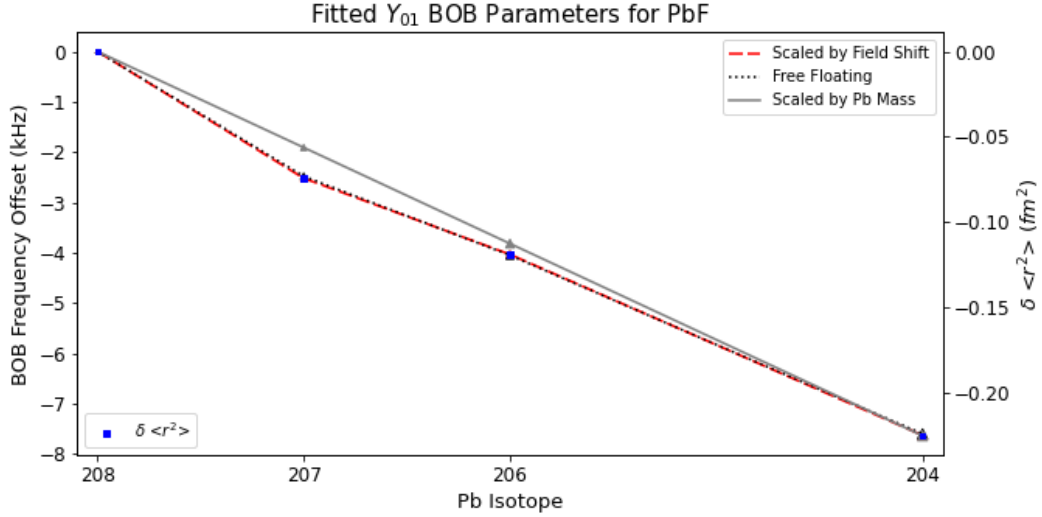


FIG. 3. Plotted frequency offsets to Y_{01} vs. Pb isotope for three different cases. The black dotted line shows the BOB frequency offsets for each isotopologue when determined separately in the fit and free to move to the best fit value. Note the excellent agreement of the free-floating BOB frequency offsets and those scaled by $\delta \langle r^2 \rangle$ values, opposed to those scaled by the Pb isotope mass. The mean square radii changes from the ^{208}PbF reference isotopologue shown in blue are from [62]. Errors are the same size as point markers.

adiabatic, and nonadiabatic terms [52, 57]. As is the case in the detailed discussion for PbO, it usually requires some assumptions to determine all 3. For an open shell molecule like PbF, the presence of the unpaired electron prevents reliably estimating the rotational g -factor, g_J , in the nonadiabatic term, which makes up 95% of the overall Δ_{01}^{Pb} term for PbO [57]. Another approach is to calculate the field shift term. The illuminating study by Knecht and Saue[55] shows that non-relativistic calculations are completely inadequate, and that extensive relativistic calculations provide agreement with experiment values at the 10-20% level.

Nevertheless, we can use the multiple alternate fits reported with either $\Delta_{01}^{Pb} \equiv 0$ [52] or $V_X \equiv 0$ [53, 57, 63] to draw a fairly clear picture of the relative importance of these terms. Table V summarizes V_X values from these studies for PbY (Y = Se, Te, S, O) and TIY (Y = F, Cl, Br, I) alongside our current PbF result. The more recent V_{Pb} results[63] for PbSe

and PbTe agree nicely, and estimates ranging from 10% to 16% for the relative fraction of Δ_{01}^{Pb} character in the 4 lead chalcogenides are also included. These have been derived by noting the consistent and very large factor of 6 to 10 jumps in the Δ_{01}^{Pb} term when the field shift term is excluded in studies of PbSe and PbTe [63], PbS [52, 53] and PbO [57]. Units of $1/\text{fm}^2$ are used to match the fm^2 units of $\delta\langle r^2 \rangle$. The alternative approach is to exclude the mass-dependent term, which Schlembach and Tiemann used in their original study for PbSe, PbTe, and PbS as well as for TlF, TlCl, TlBr, and TlI [52]. They found that this limiting case results only in changes in V_X of less than 2σ for each PbY molecule and less than 1σ for the whole TIY set.

The amount of mass-dependent character is smaller for PbS and PbO than for PbSe and PbTe, and this can be understood both in terms of the smaller sizes of S and O atoms as well as their increasing electronegativity due to the physical dependence of V_X on the derivative $d\rho/dr$ of the charge density at the nucleus [57, 63]. For PbF, fluorine is small and even more electronegative, and indeed our reported V_{Pb} value of $48.8(20) \times 10^{-7} \text{ fm}^{-2}$ is closer to that found for the more ionic TIY molecules, where it ranges from 32.0 to $40.9 \times 10^{-7} \text{ fm}^{-2}$ from TlI to TlF. Our PbF value assumes $\Delta_{01}^{Pb} \equiv 0$ and the alternate V_{Pb} only fit shown in Figure 3 validates this assumption. While we are unable to reliably estimate it, we are confident Δ_{01}^{Pb} is quite small. To estimate an uncertainty, based on Schlembach and Tiemann's experience with $\Delta_{01}^X \equiv 0$ analyses [52], we use their 1σ value of $1.9 \times 10^{-7} \text{ fm}^{-2}$ for the most similar case of TlF and add it in quadrature with our much smaller statistical uncertainty of $0.4 \times 10^{-7} \text{ fm}^{-2}$.

The ΔA_e parameter in Table I may be interpreted as the contribution to the electronic transition energy between X_1 and X_2 resulting from the extended size of the nucleus. If this is the case, then $d\Delta A_e/d\langle r^2 \rangle$ should be similar to the field shift factor $F = d\nu/d\langle r^2 \rangle$ (where ν is the atomic transition energy) commonly used in atomic isotope shift studies. For atoms, this parameter is considered to be constant, i.e. independent of the isotope pair. By referring to Table I and Ref. [55], we may calculate that $d\Delta A_e/d\langle r^2 \rangle(208 - 207\text{Pb}) = -2681(28) \text{ MHz}/\text{fm}^2$, and $d\Delta A_e/d\langle r^2 \rangle(208 - 206\text{Pb}) = -2624(19) \text{ MHz}/\text{fm}^2$; this seems very reasonable agreement.

For the Λ -doubling parameter p_{00} , second-order perturbation theory also shows that p_{00}

TABLE V. Born-Oppenheimer breakdown field shift parameters for Pb and Tl diatomic molecules.

Molecule	\mathbf{V}_X (10^{-7} fm $^{-2}$) ^a	Δ_{01}^{Pb} character	Reference
²⁰⁸ Pb ⁸⁰ Se	22.1(19)	-	[52]
	22.5(20)	0.15	[63]
²⁰⁸ Pb ¹³⁰ Te	21.2(16)	-	[52]
	20.7(21)	0.16	[63]
²⁰⁸ Pb ³² S	24.5(19)	-	[52]
	"	0.10	[52, 53]
²⁰⁸ Pb ¹⁶ O	26.4(36)	0.13	[57]
²⁰⁸ Pb ¹⁹ F	48.8(20) ^b	-	this work
²⁰⁵ Tl ¹⁹ F	40.9(19)	-	[52]
²⁰⁵ Tl ³⁵ Cl	40.9(55)	-	[52]
²⁰⁵ Tl ⁷⁹ Br	33.7(10)	-	[52]
²⁰⁵ Tl ¹²⁷ I	32.0(10)	-	[52]

^a All uncertainties are 1σ unless otherwise noted.

^b Assuming $\Delta_{01}^{Pb} = 0$. See text for details of the estimated uncertainty.

is proportional to $(A_{00}^{iso} \times Y_{01})/\Delta E$, with an extra factor of 2 compared with γ_{00} [46]. Indeed $p_{00} \approx -4140$ MHz is roughly a factor of 2 greater than the earlier γ_{00} estimate of -2300 MHz. Furthermore, our values of $p_{00}/(A_{00}^{iso} \times Y_{01})$ are quite constant, pointing to the overall consistency of this analysis.

Based on the above arguments, the nonlinear isotope dependence of A_{00}^{iso} will also be present in the p_{00} parameter and can be accounted for using a mass-dependent Δ_{01} BOB parameter, determined following the method described by Preston [64]. Using the relations

$$\delta_{01}^{p_{00}} = \left(\frac{p_{00}^{\alpha} + \text{offset}}{\mu^{ref}/\mu^{\alpha}} - p_{00}^{ref} \right) / \frac{M^{\alpha} - M^{ref}}{M^{\alpha}} \quad (15)$$

and

$$\Delta_{01}^{p_{00}} = -\delta_{01} \left(\frac{M^{ref}}{m_e} \right) \left[(p_{00}^{ref} + \delta_{01})^{-1} \right], \quad (16)$$

where the ‘‘offset’’ term is the frequency offset to the p_{00} term determined in the fitting, and ²⁰⁸Pb¹⁹F is used as the reference isotopologue. We find a unitless Watson-type $\Delta_{01}^{p_{00}}$ value of 99(10). This is large compared to typical values for rotational constants, but we are not aware of other published values of $\Delta_{01}^{p_{00}}$ for comparison. We also note that the BOB frequency offsets for V_{Pb} and $\Delta_{01}^{p_{00}}$ are found to be of comparable size at about -2.5 kHz and

–5 kHz respectively, while as a percentage the p_{00} BOB frequency offset is about another factor of 2 larger.

F. Sensitivity of the PbF molecule to variation of fundamental constants

This section and the next deal with the special sensitivity of PbF to symmetry-breaking effects. As already noted, Luan et al. [20] have further investigated the feasibility as well as some practical considerations of laser cooling the lead halides PbX ($X = \text{F}, \text{Cl}, \text{Br}, \text{I}$). They used relativistic methods and find quite diagonal Frank-Condon factors (FCFs) in each case. These greatly facilitate the laser cooling required to study subtle symmetry-breaking effects, and PbF is the lightest of the halides possessing the smallest level density.

Nowadays the possibility of observing the space-time variation of the fine-structure constant $\alpha = e^2/\hbar c$, the electron-to-proton mass ratio, m_e/m_p , and the dimensionless fundamental parameter for strong interactions m_q/Λ_{QCD} , where m_q is the light quark mass and Λ_{QCD} is the QCD scale, is of great interest. The parameter m_q/Λ_{QCD} enters atomic physics through nuclear magnetic g -factors [65, 66]. To date, almost all searches for space-time variation in fundamental constants have been performed on atoms, the only exception being the experiment on the rovibrational transitions of the SF₆ molecule [67].

In Ref. [68] it was noted that the existence of closely spaced levels of opposite parity also enhances the sensitivity of molecular spectra to variation of fundamental constants α and m_q/Λ_{QCD} . For variation of the frequency $\omega = E(F^p = 1/2^+) - E(F^p = 1/2^-) = 266.285$ MHz for $v = 0$ with respect to α and $(m_q/\Lambda_{\text{QCD}})$ it was found

$$\frac{\delta\omega}{\omega} \approx -55 \frac{\delta\alpha}{\alpha} + 2.1 \frac{\delta(m_q/\Lambda_{\text{QCD}})}{(m_q/\Lambda_{\text{QCD}})}. \quad (17)$$

One can see from Eq. (17) that the $^{207}\text{Pb}^{19}\text{F}$ molecular radical species can offer about two orders of magnitude (two orders means that the coefficient in front of the $\frac{\delta\alpha}{\alpha}$ in Eq. (17) is of order 10^2 .) enhancement of the relative effect of α -variation. This is comparable to the enhancements in some other molecular species [69–72]. However, the sensitivity coefficient for m_q/Λ_{QCD} is enhanced by two orders of magnitude compared with the ratio of frequencies

of ^{133}Cs and ^{87}Rb atomic clocks, which currently provide the best limit on the variation of m_q/Λ_{QCD} [73].

In general the variation of the frequency $\omega = E(F^p = 1/2^+) - E(F^p = 1/2^-)$ with respect to α and $(m_q/\Lambda_{\text{QCD}})$ can be written as

$$\frac{\partial\omega}{\partial\alpha} = \frac{\partial\omega}{\partial p} \frac{\partial p}{\partial\alpha} + \frac{\partial\omega}{\partial A_{\parallel}^{Pb}} \frac{\partial A_{\parallel}^{Pb}}{\partial\alpha} + \frac{\partial\omega}{\partial A_{\perp}^{Pb}} \frac{\partial A_{\perp}^{Pb}}{\partial\alpha}, \quad (18)$$

$$\frac{\partial\omega}{\partial(m_q/\Lambda_{\text{QCD}})} = \frac{\partial\omega}{\partial A_{\parallel}^{Pb}} \frac{\partial A_{\parallel}^{Pb}}{\partial(m_q/\Lambda_{\text{QCD}})} + \frac{\partial\omega}{\partial A_{\perp}^{Pb}} \frac{\partial A_{\perp}^{Pb}}{\partial(m_q/\Lambda_{\text{QCD}})}. \quad (19)$$

For the X_1 component, the A_{\parallel} and A_{\perp} parameters are defined in section V C. From the results of Flambaum et al. [68], we can show

$$\frac{\partial p}{\partial\alpha} = 2.1538p/\alpha, \quad (20)$$

$$\frac{\partial A_{\parallel}^{Pb}}{\partial\alpha} = 4.39A_{\parallel}^{Pb}/\alpha, \quad (21)$$

$$\frac{\partial A_{\perp}^{Pb}}{\partial\alpha} = 4.39A_{\perp}^{Pb}/\alpha, \quad (22)$$

$$\frac{\partial A_{\parallel}^{Pb}}{\partial(m_q/\Lambda_{\text{QCD}})} = -0.111A_{\parallel}^{Pb}/(m_q/\Lambda_{\text{QCD}}), \quad (23)$$

$$\frac{\partial A_{\perp}^{Pb}}{\partial(m_q/\Lambda_{\text{QCD}})} = -0.111A_{\perp}^{Pb}/(m_q/\Lambda_{\text{QCD}}). \quad (24)$$

According to the present calculations:

$$\frac{\partial\omega}{\partial p} = -0.838, \quad (25)$$

$$\frac{\partial\omega}{\partial A_{\parallel}^{Pb}} = -0.153, \quad (26)$$

$$\frac{\partial\omega}{\partial A_{\perp}^{Pb}} = +0.507, \quad (27)$$

for $v = 7$ and:

$$\frac{\partial\omega}{\partial p} = +0.835, \quad (28)$$

$$\frac{\partial\omega}{\partial A_{\parallel}^{Pb}} = +0.154, \quad (29)$$

$$\frac{\partial\omega}{\partial A_{\perp}^{Pb}} = -0.509. \quad (30)$$

for $v = 8$.

Combining Eqs. (20)-(30) we have

$$\frac{\delta\omega}{\omega} \approx -720 \frac{\delta\alpha}{\alpha} + 27 \frac{\delta(m_q/\Lambda_{QCD})}{(m_q/\Lambda_{QCD})} \quad (31)$$

for $v = 7$ and

$$\frac{\delta\omega}{\omega} \approx 1084 \frac{\delta\alpha}{\alpha} - 39 \frac{\delta(m_q/\Lambda_{QCD})}{(m_q/\Lambda_{QCD})} \quad (32)$$

for $v = 8$.

One can see from Eqs. (17, 31, 32) that the $v = 7$ and $v = 8$ vibrational levels offer a further enhancement about one order of magnitude higher as compared to the $v = 0$ level.

We note, that the corresponding absolute values for the frequencies shifts

$$\frac{\delta\omega}{\text{GHz}} \approx -15 \frac{\delta\alpha}{\alpha} + 0.56 \frac{\delta(m_q/\Lambda_{QCD})}{(m_q/\Lambda_{QCD})} \quad (33)$$

for $v = 0$,

$$\frac{\delta\omega}{\text{GHz}} \approx -16 \frac{\delta\alpha}{\alpha} + 0.61 \frac{\delta(m_q/\Lambda_{QCD})}{(m_q/\Lambda_{QCD})} \quad (34)$$

for $v = 7$ and

$$\frac{\delta\omega}{\text{GHz}} \approx -16 \frac{\delta\alpha}{\alpha} + 0.59 \frac{\delta(m_q/\Lambda_{QCD})}{(m_q/\Lambda_{QCD})} \quad (35)$$

for $v = 8$ are about the same (Note (see Table IV), that the frequency ω for $v = 8$ is assumed to be negative). From Eqs. (31,32) one can see that the sensitivity coefficients for the $v = 7$ and $v = 8$ levels have opposite signs that could be a powerful tool for suppressing possible systematic errors. Coefficients in fronts of $\frac{\delta\alpha}{\alpha}$ and $\frac{\delta(m_q/\Lambda_{QCD})}{(m_q/\Lambda_{QCD})}$ scale very similarly for different transitions. Therefore, unfortunately, it is difficult for an experiment to differentiate between variations of fundamental constants using only the PbF molecule.

G. Sensitivity of the PbF molecule to the electron electric dipole moment

In a polar molecule the \mathcal{T} , \mathcal{P} -violating energy shift associated with e EDM reads

$$\Delta E_{\mathcal{P},\mathcal{T}} = P E_{\text{eff}} d_e, \quad (36)$$

where d_e is the value of the e EDM, E_{eff} is effective electric field determined by the electronic structure of the molecule, and P is the corresponding \mathcal{P} , \mathcal{T} -odd polarization coefficient. In Ref. [74] we calculated that $E_{\text{eff}} = 40$ GV/cm.

It is well known that for $\Omega = 1$ diatomics (such as HfF⁺ and ThO), due to the existence of the Ω -doublet structure, the P value approaches unity for small ($\sim 10 - 100$ V/cm) laboratory electric fields. In general, for $\Omega = 1/2$ diatomics a much larger electric field is required because the parity doublets are further apart in energy. For example for the YbF molecule in the ground $^2\Sigma_{1/2}$ state P is only 0.55 for $E = 10$ kV/cm [75]. For $^{206,208}\text{PbF}$ (spin-less even isotopes of Pb) at $E = 5$ kV/cm the polarisation is about 80% [17].

Due to the accidental near cancellation of the Ω -type doubling and magnetic hyperfine interaction energy shifts, the situation is different for ^{207}PbF . In this case the energy spacing between levels of opposite parity is much smaller than the typical value for $\Omega = 1/2$ diatomics. The latter makes the molecule more promising for the e EDM search experiment. Figure 1 of [6] shows the hyperfine split levels of interest for $v = 0$. The energy levels of interest for an e EDM search experiment on ^{207}PbF are those from the second to the fifth close Ω -doublets levels $F^p = 3/2^-$, $F^p = 1/2^-$, $F^p = 1/2^+$ and $F^p = 3/2^+$ associated with $J = 1/2$ in the figure.

As calculated in Ref. [17] ^{207}PbF as compared to $^{206,208}\text{PbF}$ can be polarized by a smaller electric field, which is an advantage since larger electric field tends to lead to larger systematic effects. For example for ^{207}PbF $F = 3/2$, $|M_F|=3/2$, $v = 0$, $P = 0.8$ polarization is achieved for $E = 1$ kV/cm. For $E = 2$ kV/cm, P is about 90%.

In Fig. 4 the calculated polarization P for $v = 7$ and $v = 8$ are shown. For ^{207}PbF

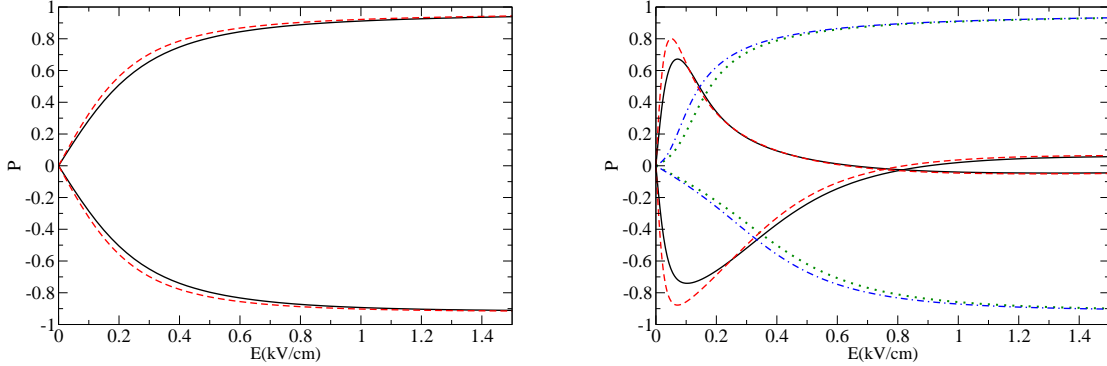


FIG. 4. Left: Calculated polarization P as function of the electric field E for $F = 3/2$ $M_F = 3/2$. Solid (black) lines correspond to $v = 7$, dashed (red) lines correspond to $v = 8$ vibrational levels. Ω -doublets levels marked by the same colour. Right: Calculated polarization P as function of the electric field E . Solid (black) lines correspond to $F = 1/2$ $M_F = 1/2$ $v = 7$, dashed (red) lines correspond to $F = 1/2$ $M_F = 1/2$ $v = 8$, dotted (green) lines correspond to $F = 3/2$ $M_F = 1/2$ $v = 7$, dashed-dotted (blue) lines correspond to $F = 3/2$ $M_F = 1/2$ $v = 8$. Ω -doublets levels marked by the same colour.

$F = 3/2$, $|M_F|=3/2$, $P = 0.9$ is achieved for $E = 1$ kV/cm for both $v = 7$ and $v = 8$ levels. For ^{207}PbF $F = 1/2$, $|M_F|=1/2$, $v = 8$ we already have $P = -0.9$ for an electric field less than 100 V/cm.

VI. CONCLUSIONS

Lead monofluoride is a strong molecular candidate for current and future investigations of the role of parity non-conservation in theories beyond the standard model, as well as in hunting for the extra parity non-conservation, PNC, effects needed to explain the observed fundamental matter-antimatter baryon asymmetry in the universe. We also show that PbF may be a useful vehicle for investigating possible time variation of the fundamental constants and a better understanding of the spin-dependent nuclear PNC effect known as the anapole moment.

The present results offer a great deal of information needed for further investigation of these effects, for example complementing the several ongoing studies of the eEDM. The ground state sensitivity of ^{207}PbF to PNC effects is optimized by the near-degeneracy of

opposite parity states in the $v = 8$ level, where they are found to be only 15 MHz apart. Importantly, we find that the lifetime of this level is 38 ms, long enough for proposed optical cooling experiments [20] to be employed and also longer than the typical transit time limitations in beam measurements of buffer gas-cooled samples [76]. The isotopically independent parameters describing the coupled X_1 / X_2 states of the molecule determined here have resulted in a much more accurate picture of their properties. Highlights of the results include:

- The new high resolution $X_2, v = 1 - X_1, v = 1$ NIR data and an improved model to account for isotopic shifts has resulted in a much clearer picture of the X_1 and X_2 spin-orbit split molecular potentials.
- Born-Oppenheimer breakdown (BOB) effects in both the rotation constant Y_{01} and the lambda-doubling constant p_{00} have been observed and accounted for. A simple single perturbing state model finds that p is proportional to $(A \times Y_{01})$, and this closely mimics the results. Hence the isotopic dependence observed for p_{00} can be traced back to that in A_e and the $X_1 - X_2$ energy spacing discussed above.
- The rich isotopic data set has enabled a separation of the effects of the centrifugal distortion correction to the spin-orbit term A_{01} and the electron spin-nuclear rotation interaction γ that usually result in indistinguishable contributions to the energy.
- A comparison with other PbX and TIY BOB studies showed that essentially all of the Y_{01} BOB effect is due to the finite nuclear size of Pb, and the measured residuals match the trend in nuclear sizes almost exactly.
- The case for the sensitivity of PbF to the variation of fundamental constants has been augmented as well as the primary eEDM sensitivity noted above.

Future work could entail further excited state characterization based on laser spectroscopy of the $X_2 - X_1$ band system in a cooled sample which could resolve remaining ambiguities in the hyperfine splittings in the upper component, as well as work to experimentally test the laser slowing theory posited recently [20]. Both would be a good further steps towards realizing the full potential of PbF for molecular PNC investigations and possible studies of the time variation of fundamental constants put forward here.

VII. ACKNOWLEDGEMENTS

The Pomona College authors thank fellow student José Muñoz-Lopez for assistance taking data. They also appreciate research support provided by a Pomona College Sontag Fellowship as well as Hirsch Research Initiation and Summer Undergraduate Research Program grants. Ewald Fink and Klaus Setzer from Wuppertal are acknowledged for kindly sharing their unpublished $v = 1 - 1$ data. TJS acknowledges support by the U.S. Department of Energy, Office of Science, Division of Chemical Sciences, Geosciences and Biosciences within the Office of Basic Energy Sciences, under Award Number DE-SC0018950 for part of this work. JUG acknowledges support from the Deutsche Forschungsgemeinschaft (DFG) under GR1344/11-1 and from the Land Niedersachsen. Calculations of sensitivity to variation of fundamental constants and to electron electric dipole moment are supported by the Russian Science Foundation grant no. 24-12-00092.

-
- [1] L. N. Labzovsky, Λ doubling and parity nonconservation effects in the spectra of diatomic molecules, *Sov. Phys.–JETP* **48**, 434 (1978).
- [2] V. G. Gorshkov, L. N. Labzovsky, and A. N. Moskalyov, Space and time parity nonconservation effects in the spectra of diatomic molecules, *Sov. Phys.–JETP* **49**, 209 (1979).
- [3] O. P. Sushkov and V. V. Flambaum, Parity violation effects in diatomic molecules, *Sov. Phys.–JETP* **48**, 608 (1978).
- [4] M. G. Kozlov, V. I. Fomichev, Y. Y. Dmitriev, L. N. Labzovsky, and A. V. Titov, Calculation of the P- and T-odd spin-rotational Hamiltonian of the PbF molecule, *J. Phys. B* **20**, 4939 (1987), [Preprint LNPI 1228 (Leningrad, 1986)].
- [5] C. P. McRaven, P. Sivakumar, and N. E. Shafer-Ray, Experimental determination of the hyperfine constants of the X_1 and A states of $^{207}\text{Pb}^{19}\text{F}$, *Phys. Rev. A* **78**, 054502(R) (2008), erratum: *Phys. Rev. A* **80**, 029902(E) (2009).
- [6] R. J. Mawhorter, B. S. Murphy, A. L. Baum, T. J. Sears, T. Yang, P. M. Rupasinghe, C. P. McRaven, N. E. Shafer-Ray, L. D. Alpei, and J.-U. Grabow, Characterization of the ground X_1 state of $^{204}\text{Pb}^{19}\text{F}$, $^{206}\text{Pb}^{19}\text{F}$, $^{207}\text{Pb}^{19}\text{F}$, and $^{208}\text{Pb}^{19}\text{F}$, *Phys. Rev. A* **84**, 022508 (2011).
- [7] I. Kozyryev and N. R. Hutzler, Precision measurement of time-reversal symmetry violation with laser-cooled polyatomic molecules, *Phys. Rev. Lett.* **119**, 133002 (2017).
- [8] A. Petrov and A. Zakharova, Sensitivity of the YbOH molecule to \mathcal{PT} -odd effects in an external electric field, *Phys. Rev. A* **105**, L050801 (2022).
- [9] A. Jadbabaie, Y. Takahashi, N. H. Pilgram, C. J. Conn, Y. Zeng, C. Zhang, and N. R. Hutzler, Characterizing the fundamental bending vibration of a linear polyatomic molecule for symmetry violation searches, *New J. Phys.* **25**, 073014 (2023).
- [10] A. Petrov, Electronic matrix elements for parity doubling in the YbOH molecule, *Phys. Rev. A* **109**, 012819 (2024).
- [11] L. D. Alpei, J.-U. Grabow, A. N. Petrov, R. Mawhorter, B. Murphy, A. Baum, T. J. Sears, T. Z. Yang, P. M. Rupasinghe, C. P. McRaven, and N. E. Shafer-Ray, Precision spectroscopy of the $^{207}\text{Pb}^{19}\text{F}$ molecule: Implications for measurement of P -odd and T -odd effects, *Phys. Rev. A* **83**, 040501 (2011).

- [12] A. N. Petrov, L. V. Skripnikov, A. V. Titov, and R. J. Mawhorter, Centrifugal correction to hyperfine structure constants in the ground state of lead monofluoride, *Phys. Rev. A* **88**, 010501 (2013).
- [13] L. V. Skripnikov, A. N. Petrov, A. V. Titov, R. J. Mawhorter, A. L. Baum, T. J. Sears, and J.-U. Grabow, Further investigation of g factors for the lead monofluoride ground state, *Phys. Rev. A* **92**, 032508 (2015).
- [14] T. S. Roussy, L. Caldwell, T. Wright, W. B. Cairncross, Y. Shagam, K. B. Ng, N. Schlossberger, S. Y. Park, A. Wang, J. Ye, and E. A. Cornell, An improved bound on the electrons electric dipole moment, *Science* **381**, 46 (2023), <https://www.science.org/doi/pdf/10.1126/science.adg4084>.
- [15] V. Andreev, D. Ang, D. DeMille, J. Doyle, G. Gabrielse, J. Haefner, N. Hutzler, Z. Lasner, C. Meisenhelder, B. O’Leary, *et al.*, Improved limit on the electric dipole moment of the electron, *Nature* **562**, 355 (2018).
- [16] D. DeMille, F. Bay, S. Bickman, D. Kawall, L. Hunter, D. Krause, S. Maxwell, and K. Ulmer, Search for the electric dipole moment of the electron using metastable PbO, in *AIP Conference Proceedings*, Vol. 596 (AIP, 2001) pp. 72–83.
- [17] V. V. Baturo, P. M. Rupasinghe, T. J. Sears, R. J. Mawhorter, J.-U. Grabow, and A. N. Petrov, Electric-field-dependent g factor for the ground state of lead monofluoride, PbF, *Phys. Rev. A* **104**, 012811 (2021).
- [18] R. Mawhorter, J. Munoz-Lopez, Y. Kim, A. Biekert, T. Sears, J.-U. Grabow, A. D. Kudashov, L. V. Skripnikov, A. V. Titov, and A. N. Petrov, ^{207}PbF near-degeneracy and BaF microwave global fit (<http://meetings.aps.org/link/BAPS.2018.DAMOP.E01.81>, 2018).
- [19] V. V. Flambaum, Y. V. Stadnik, M. G. Kozlov, and A. N. Petrov, Enhanced effects of temporal variation of the fundamental constants in $^2\Pi_{1/2}$ -term diatomic molecules- $^{207}\text{Pb}^{19}\text{F}$, *Phys. Rev. A* **88**, 052124 (2013).
- [20] J.-Z. Luan, C.-L. Yang, X. Li, W.-W. Liu, Y.-L. Liu, and W.-K. Zhao, Spectroscopic properties and laser cooling feasibility with the $X_1\ ^2\Pi_{1/2} \leftrightarrow X_2\ ^2\Pi_{3/2}$ transition for the PbX (X = F, Cl, Br, and I) molecules, *Physica Scripta* **99**, 035406 (2024).
- [21] C. Zhu, H. Wang, B. Chen, Y. Chen, T. Yang, J. Yin, and J. Liu, Fine and hyperfine interactions of PbF studied by laser-induced fluorescence spectroscopy, *J. Chem. Phys.* **157**, 084307 (2022), <https://pubs.aip.org/aip/jcp/article->

- pdf/doi/10.1063/5.0099716/16550822/084307_1_online.pdf.
- [22] K. Ziebarth, K. D. Setzer, O. Shestakov, and E. H. Fink, High-Resolution Study of the $X_2^2\Pi_{3/2} - X_1^2\Pi_{1/2}$ Fine Structure Transitions of PbF and PbCl, *J. Mol. Spectrosc.* **191**, 108 (1998).
- [23] S. Jackson, Using spectroscopy of diatomic molecules to search for physics beyond the standard model (2023), https://scholarship.claremont.edu/pomona_theses/320/.
- [24] J. Grabow, W. Stahl, and H. Dreizler, A multioctave coaxially oriented beam-resonator arrangement Fourier-transform microwave spectrometer, *Review of Scientific Instruments* **67**, 4072 (1996), https://pubs.aip.org/aip/rsi/article-pdf/67/12/4072/8810020/4072_1_online.pdf.
- [25] J.-U. Grabow, E. S. Palmer, M. C. McCarthy, and P. Thaddeus, Supersonic-jet cryogenic-resonator coaxially oriented beam-resonator arrangement Fourier transform microwave spectrometer, *Review of Scientific Instruments* **76**, 093106 (2005), https://pubs.aip.org/aip/rsi/article-pdf/doi/10.1063/1.2039347/15829418/093106_1_online.pdf.
- [26] L. Bizzocchi, B. M. Giuliano, M. Hess, and J.-U. Grabow, The rotational spectra, potential function, born-oppenheimer breakdown, and magnetic shielding of snse and snse, *J. Chem. Phys.* **126**, 114305 (2007).
- [27] R. J. Bartlett and M. Musiał, Coupled-cluster theory in quantum chemistry, *Rev. Mod. Phys.* **79**, 291 (2007).
- [28] L. Visscher, T. J. Lee, and K. G. Dyall, Formulation and implementation of a relativistic unrestricted coupled-cluster method including noniterative connected triples, *J. Chem. Phys.* **105**, 8769 (1996).
- [29] A. V. Titov and N. S. Mosyagin, Generalized relativistic effective core potential: Theoretical grounds, *Int. J. Quant. Chem.* **71**, 359 (1999).
- [30] N. S. Mosyagin, A. V. Zaitsevskii, and A. V. Titov, Shape-consistent relativistic effective potentials of small atomic cores, *Int. Rev. At. Mol. Phys* **1**, 63 (2010).
- [31] N. S. Mosyagin, A. V. Zaitsevskii, L. V. Skripnikov, and A. V. Titov, Generalized relativistic effective core potentials for actinides, *Int. J. Quant. Chem.* **116**, 301 (2016).
- [32] L. V. Skripnikov, N. S. Mosyagin, and A. V. Titov, Relativistic coupled-cluster calculations of spectroscopic and chemical properties for element 120, *Chem Phys. Lett.* **555**, 79 (2013).

- [33] K. G. Dyall, Relativistic double-zeta, triple-zeta, and quadruple-zeta basis sets for the light elements H–Ar, *Theor. Chem. Acc.* **135**, 128 (2016).
- [34] (2019), *DIRAC*, a relativistic ab initio electronic structure program, Release DIRAC19 (2019), written by A. S. P. Gomes, T. Saue, L. Visscher, H. J. Aa. Jensen, and R. Bast, with contributions from I. A. Aucar, V. Bakken, K. G. Dyall, S. Dubillard, U. Ekstroem, E. Eliav, T. Enevoldsen, E. Fasshauer, T. Fleig, O. Fossgaard, L. Halbert, E. D. Hedegaard, T. Helgaker, J. Henriksson, M. Ilias, Ch. R. Jacob, S. Knecht, S. Komorovsky, O. Kullie, J. K. Laerdahl, C. V. Larsen, Y. S. Lee, H. S. Nataraj, M. K. Nayak, P. Norman, M. Olejniczak, J. Olsen, J. M. H. Olsen, Y. C. Park, J. K. Pedersen, M. Pernpointner, R. Di Remigio, K. Ruud, P. Salek, B. Schimmelpfennig, B. Senjean, A. Shee, J. Sikkema, A. J. Thorvaldsen, J. Thyssen, J. van Stralen, M. L. Vidal, S. Villaume, O. Visser, T. Winther, and S. Yamamoto (see <http://diracprogram.org>).
- [35] T. Saue, R. Bast, A. S. P. Gomes, H. J. A. Jensen, L. Visscher, I. A. Aucar, R. Di Remigio, K. G. Dyall, E. Eliav, E. Fasshauer, T. Fleig, L. Halbert, E. D. Hedegard, B. Helmich-Paris, M. Ilias, C. R. Jacob, S. Knecht, J. K. Laerdahl, M. L. Vidal, M. K. Nayak, M. Olejniczak, J. M. H. Olsen, M. Pernpointner, B. Senjean, A. Shee, A. Sunaga, and J. N. P. van Stralen, The dirac code for relativistic molecular calculations, *J. Chem. Phys.* **152**, 204104 (2020).
- [36] MRCC, m. Kállay, P. R. Nagy, D. Mester, Z. Rolik, G. Samu, J. Csontos, J. Csóka, P. B. Szabó, L. Gyevi-Nagy, B. Hégyely, I. Ladjánszki, L. Szegedy, B. Ladóczki, K. Petrov, M. Farkas, P. D. Mezei, and á. Ganyecz: The MRCC program system: Accurate quantum chemistry from water to proteins, *J. Chem. Phys.* **152**, 074107 (2020); MRCC, a quantum chemical program suite written by M. Kállay, P. R. Nagy, D. Mester, Z. Rolik, G. Samu, J. Csontos, J. Csóka, P. B. Szabó, L. Gyevi-Nagy, B. Hégyely, I. Ladjánszki, L. Szegedy, B. Ladóczki, K. Petrov, M. Farkas, P. D. Mezei, and Á. Ganyecz. See www.mrcc.hu.
- [37] M. Kállay and P. R. Surján, Higher excitations in coupled-cluster theory, *J. Chem. Phys.* **115**, 2945 (2001).
- [38] M. Kállay, P. G. Szalay, and P. R. Surján, A general state-selective multireference coupled-cluster algorithm, *J. Chem. Phys.* **117**, 980 (2002).
- [39] K. Ziebarth, R. Breidohr, O. Shestakov, and E. Fink, The $X_2 - X_1$ electronic band systems of lead monohalides in the near infrared, *Chemical Physics Letters* **190**, 271 (1992).

- [40] H. M. Pickett, The fitting and prediction of vibration-rotation spectra with spin interactions, *Journal of Molecular Spectroscopy* **148**, 371 (1991).
- [41] S. E. Novick, A beginner’s guide to Pickett’s SPCAT/SPFIT, *Journal of Molecular Spectroscopy* **329**, 1 (2016).
- [42] R. B. Shirts, Connecting the Dunham Expansion to the Dissociation Limit for Interatomic Potentials: Application to Lennard-Jones $m-n$ Potentials, *J. Phys. Chem. A* **122**, 8591 (2018), PMID: 30296094, <https://doi.org/10.1021/acs.jpca.8b08095>.
- [43] W. Gordy and R. L. Cook, *Techniques of Chemistry, Microwave Molecular Spectra*, Techniques of Chemistry (Wiley, 1984).
- [44] B. Drouin, C. Miller, H. Muller, and E. Cohen, The rotational spectra, isotopically independent parameters, and interatomic potentials for the $X_1^2\Pi_{3/2}$ and $X_2^2\Pi_{1/2}$ states of BrO, *J. Molec. Spectrosc.* **205**, 128 (2001).
- [45] R. A. Frosch and H. M. Foley, Magnetic hyperfine structure in diatomic molecules, *Phys. Rev* **88**, 1337 (1952).
- [46] J. M. Brown and A. Carrington, *Rotational Spectroscopy of Diatomic Molecules*, Cambridge Molecular Science (Cambridge University Press, 2003).
- [47] E. Cohen, D. Goodridge, K. Kawaguchi, E. Fink, and K. Setzer, The rotational spectrum of BiO radical in its $X_1^2\Pi_{1/2}$ and $X_2^2\Pi_{3/2}$ states, *Journal of Molecular Spectroscopy* **239**, 16 (2006).
- [48] D. J. W. Lumley and R. F. Barrow, Rotational analysis of $B-X_2$, $B-X_1$ and $A-X_1$ systems of gaseous PbF, *J. Phys. B-Atom. Molec. Opt. Phys.* **10**, 1537 (1977).
- [49] K. P. Huber and G. Herzberg, Constants of diatomic molecules, in *Molecular Spectra and Molecular Structure: IV. Constants of Diatomic Molecules* (Springer US, Boston, MA, 1979) pp. 8–689, <https://webbook.nist.gov/cgi/cbook.cgi?ID=C14986722>.
- [50] J. M. Brown and J. K. G. Watson, Spin-orbit and spin-rotation coupling in doublet states of diatomic-molecules, *J. Molec. Spectrosc.* **65**, 65 (1977).
- [51] C. P. McRaven, P. Sivakumar, N. E. Shafer-Ray, G. E. Hall, and T. J. Sears, Spectroscopic constants of the known electronic states of lead monofluoride, *J. Molec. Spectrosc.* **262**, 89 (2010).
- [52] J. Schlembach and E. Tiemann, Isotopic field shift of the rotational energy of the Pb-chalcogenides and Tl-halides, *Chem. Phys.* **68**, 21 (1982).

- [53] E. Tiemann, H. Arnst, W. Stieda, T. Törring, and J. Hoeft, Observed adiabatic corrections to the born-oppenheimer approximation for diatomic molecules with ten valence electrons, *Chem. Phys.* **67**, 133 (1982).
- [54] J. K. Watson, The isotope dependence of diatomic dunham coefficients, *J. Molec. Spectrosc.* **80**, 411 (1980).
- [55] S. Knecht and T. Saue, Nuclear size effects in rotational spectra: A tale with a twist, *Chemical Physics* **401**, 103 (2012), recent advances in electron correlation methods and applications.
- [56] A. Almoukhalalati, A. Shee, and T. Saue, Nuclear size effects in vibrational spectra, *Phys. Chem. Chem. Phys.* **18**, 15406 (2016).
- [57] M. Serafin, S. Peebles, C. Dewberry, K. Etchison, G. Grubbs, R. Powoski, and S. Cooke, Concerning the electron density at the Pb nucleus in PbO as a function of bond length, *Chemical Physics Letters* **449**, 33 (2007).
- [58] H. Knöckel, T. Kröckertskothén, and E. Tiemann, Molecular-beam-laser studies of the states $X^1\Sigma^+$ and $A0^+$ of PbS, *Chemical Physics* **93**, 349 (1985).
- [59] E. Tiemann, Private communication, (2022).
- [60] A. Preston, S. Jackson, and R. Mawhorter, Global rovibrational fits for AlCl, BiCl, and BiF: Benchmarks for novel physics, *Chemical Physics Letters* **807**, 140089 (2022).
- [61] A. Preston, G. Aufderheide, W. Ballard, R. A. Mawhorter, and J.-U. Grabow, The rotational spectrum of barium fluoride, BaF, by Fouier-transform microwave spectroscopy, *Phys. Rev. A* (2024), in preparation.
- [62] I. Angeli and K. Marinova, Table of experimental nuclear ground state charge radii: An update, *Atomic Data and Nuclear Data Tables* **99**, 69 (2013).
- [63] B. M. Giuliano, L. Bizzocchi, S. Cooke, D. Banser, M. Hess, J. Fritzsche, and J.-U. Grabow, Pure rotational spectra of PbSe and PbTe: potential function, Born–Oppenheimer breakdown, field shift effect and magnetic shielding, *Phys. Chem. Chem. Phys.* **10**, 2078 (2008).
- [64] A. Preston, *Molecular Spectroscopy for Innovative Physics: AlCl and BaF* (2021), soon to be available at <https://example.com/thesis.pdf>.
- [65] V. V. Flambaum, D. B. Leinweber, A. W. Thomas, and R. D. Young, Limits on variations of the quark masses, QCD scale, and fine structure constant, *Phys. Rev. D* **69**, 115006 (2004).
- [66] V. V. Flambaum and A. F. Tedesco, Dependence of nuclear magnetic moments on quark masses and limits on temporal variation of fundamental constants from atomic clock experi-

- ments, Phys. Rev. C **73**, 055501 (2006).
- [67] A. Shelkownikov, R. J. Butcher, C. Chardonnet, and A. Amy-Klein, Stability of the Proton-to-Electron Mass Ratio, Phys. Rev. Lett. **100**, 150801 (2008).
- [68] V. V. Flambaum, Y. V. Stadnik, M. G. Kozlov, and A. N. Petrov, Enhanced effects of temporal variation of the fundamental constants in $^2\Pi_{1/2}$ -term diatomic molecules : $^{207}\text{Pb}^{19}\text{F}$, Phys. Rev. A **88**, 052124 (2013).
- [69] V. V. Flambaum, Enhanced effect of temporal variation of the fine-structure constant in diatomic molecules, Phys. Rev. A **73**, 034101 (2006).
- [70] V. V. Flambaum and M. G. Kozlov, Enhanced Sensitivity to the Time Variation of the Fine-Structure Constant and m_p/m_e in Diatomic Molecules, Phys. Rev. Lett. **99**, 150801 (2007).
- [71] D. DeMille, S. Sainis, J. Sage, T. Bergeman, S. Kotochigova, and E. Tiesinga, Enhanced Sensitivity to Variation of m_e/m_p in Molecular Spectra, Phys. Rev. Lett. **100**, 043202 (2008).
- [72] T. Zelevinsky, S. Kotochigova, and J. Ye, Precision Test of Mass-Ratio Variations with Lattice-Confined Ultracold Molecules, Phys. Rev. Lett. **100**, 043201 (2008).
- [73] J. Guéna, M. Abgrall, D. Rovera, P. Rosenbusch, M. E. Tobar, P. Laurent, A. Clairon, and S. Bize, Improved Tests of Local Position Invariance Using ^{87}Rb and ^{133}Cs Fountains, Phys. Rev. Lett. **109**, 080801 (2012).
- [74] L. V. Skripnikov, A. D. Kudashov, A. N. Petrov, and A. V. Titov, Search for parity- and time-and-parity-violation effects in lead monofluoride (PbF): *Ab initio* molecular study, Phys. Rev. A **90**, 064501 (2014).
- [75] M. R. Tarbutt, B. E. Sauer, J. J. Hudson, and E. a. Hinds, Design for a fountain of YbF molecules to measure the electron's electric dipole moment, New Journal of Physics **15**, 053034 (2013).
- [76] N. R. Hutzler, H.-I. Lu, and J. M. Doyle, The buffer gas beam: An intense, cold, and slow source for atoms and molecules, Chemical Reviews **112**, 4803 (2012), PMID: 22571401, <https://doi.org/10.1021/cr200362u>.

Appendix A

The following table lists the observed FTMW lines of PbF used in the global fit. The quantum numbers listed appear as they do in the SPFIT program, meaning the J quantum numbers are rounded up to the nearest integer number in this table. Additionally, the isotopologues of PbF are distinguished via the v quantum number. For ^{207}PbF , $v = 0$ is listed as $v = 10$, $v = 1$ is $v = 11$, and so on. For ^{206}PbF , $v = 0$ is listed as $v = 20$, $v = 1$ is $v = 21$, and so on. For ^{204}PbF , $v = 0$ is listed as $v = 30$.

FTMW Transitions of PbF														
N'	P'	v'	J'	F'_1	F'	N''	P''	v''	J''	F''_1	F''	Measured Freq (MHz).	Unc.	
1	1	0	1	0	0	1	-1	0	1	1	1	3922.50648	0.002	
1	1	0	1	1	1	1	-1	0	1	0	0	4194.77734	0.0007	
1	1	0	1	1	1	1	-1	0	1	1	1	4229.71764	0.003	
2	-1	0	2	1	1	2	1	0	2	1	1	8117.30169	0.001	
2	-1	0	2	1	1	2	1	0	2	2	2	8199.8478	0.0009	
2	-1	0	2	2	2	2	1	0	2	1	1	8307.51802	0.002	
2	-1	0	2	2	2	2	1	0	2	2	2	8390.06637	0.002	
3	1	0	3	2	2	3	-1	0	3	2	2	12277.68224	0.0007	
3	1	0	3	2	2	3	-1	0	3	3	3	12374.67007	0.0007	
3	1	0	3	3	3	3	-1	0	3	2	2	12443.85768	0.0007	
3	1	0	3	3	3	3	-1	0	3	3	3	12540.84651	0.0008	
4	-1	0	4	3	3	4	1	0	4	3	3	16428.51597	0.001	
4	-1	0	4	4	4	4	1	0	4	4	4	16688.49294	0.002	
2	1	0	2	2	4	1	-1	0	1	1	1	18414.58796	0.0005	
2	1	0	2	1	1	1	-1	0	1	0	0	18462.19332	0.0005	
2	1	0	2	1	1	1	-1	0	1	1	1	18497.13522	0.0005	
2	-1	0	2	2	2	1	1	0	1	1	1	22574.93438	0.0005	
2	-1	0	2	1	1	1	1	0	1	0	0	22691.9306	0.0005	
2	-1	0	2	1	1	1	1	0	1	1	1	22384.71706	0.0005	
2	1	1	2	2	2	1	-1	1	1	1	1	18280.36375	0.0005	
2	1	1	2	1	1	1	-1	1	1	0	0	18327.11545	0.0005	

FTMW Transitions of PbF													
N'	P'	v'	J'	F'_1	F'	N''	P''	v''	J''	F''_1	F''	Measured Freq (MHz).	Unc.
2	1	1	2	1	1	1	-1	1	1	1	1	18364.30561	0.0015
2	-1	1	2	1	1	1	1	1	1	1	1	22251.82489	0.0005
2	-1	1	2	2	2	1	1	1	1	1	1	22442.64603	0.0005
2	-1	1	2	1	1	1	1	1	1	0	0	22559.29702	0.0005
2	1	2	2	2	2	1	-1	2	1	1	1	18146.86588	0.0005
2	1	2	2	1	1	1	-1	2	1	0	0	18192.7778	0.0005
2	1	2	2	1	1	1	-1	2	1	1	1	18232.1757	0.0005
2	-1	2	2	1	1	1	1	2	1	1	1	22119.19787	0.0005
2	-1	2	2	2	2	1	1	2	1	1	1	22310.60552	0.0005
2	-1	2	2	1	1	1	1	2	1	0	0	22426.91413	0.001
2	1	3	2	1	1	1	-1	3	1	0	0	18059.1839	0.001
2	1	3	2	2	2	1	-1	3	1	1	1	18014.09752	0.0005
2	1	3	2	1	1	1	-1	3	1	1	1	18100.74795	0.0005
2	-1	3	2	1	1	1	1	3	1	1	1	21986.83747	0.001
2	-1	3	2	2	2	1	1	3	1	1	1	22178.81699	0.0005
2	1	4	2	2	2	1	-1	4	1	1	1	17882.06356	0.0005
2	1	4	2	1	1	1	-1	4	1	0	0	17926.33965	0.0005
2	-1	4	2	1	1	1	1	4	1	1	1	21854.74595	0.0005
2	-1	4	2	2	2	1	1	4	1	1	1	22047.28122	0.0007
2	1	5	2	2	2	1	-1	5	1	1	1	17750.76424	0.0005
2	1	5	2	1	1	1	-1	5	1	0	0	17794.24209	0.0005
2	-1	5	2	2	2	1	1	5	1	1	1	21916.00098	0.0005
2	1	6	2	2	2	1	-1	6	1	1	1	17620.20372	0.0005
2	-1	6	2	2	2	1	1	6	1	1	1	21784.97929	0.0005
2	1	7	2	2	2	1	-1	7	1	1	1	17490.38923	0.0005
1	1	10	1	0	1	1	-1	10	1	1	1	3187.48749	0.002
1	1	10	1	0	1	1	-1	10	1	1	2	3219.81373	0.00075
2	-1	10	2	2	2	2	1	10	2	2	2	4455.45403	0.0025

FTMW Transitions of PbF													
N'	P'	v'	J'	F'_1	F'	N''	P''	v''	J''	F''_1	F''	Measured Freq (MHz).	Unc.
2	-1	10	2	2	3	2	1	10	2	2	3	4699.22651	0.0025
1	1	10	1	1	1	1	-1	10	1	0	1	8495.00218	0.00075
3	1	10	3	3	3	3	-1	10	3	3	3	8620.54753	0.001
1	1	10	1	1	2	1	-1	10	1	0	1	8687.20982	0.00075
2	-1	10	2	1	1	2	1	10	2	1	1	11682.52107	0.00075
2	-1	10	2	1	1	2	1	10	2	1	2	11715.3703	0.00075
2	-1	10	2	1	2	2	1	10	2	1	1	11867.64154	0.001
2	-1	10	2	1	2	2	1	10	2	1	2	11900.48704	0.00075
2	1	10	2	1	2	1	-1	10	1	1	1	14430.18298	0.00075
2	1	10	2	1	2	1	-1	10	1	1	2	14462.51043	0.00075
2	1	10	2	1	1	1	-1	10	1	1	1	14463.03111	0.00075
2	1	10	2	1	1	1	-1	10	1	1	2	14495.35797	0.00075
3	1	10	3	2	2	3	-1	10	3	2	2	15865.18882	0.00075
3	1	10	3	2	3	3	-1	10	3	2	3	16108.7271	0.00075
2	1	10	2	2	3	1	-1	10	1	1	2	18333.50131	0.00075
2	1	10	2	2	2	1	-1	10	1	1	1	18380.87112	0.00075
2	1	10	2	2	2	1	-1	10	1	1	2	18413.19816	0.00075
2	-1	10	2	2	2	1	1	10	1	1	2	22377.83416	0.00075
2	-1	10	2	2	3	1	1	10	1	1	2	22541.91225	0.00075
2	-1	10	2	2	2	1	1	10	1	1	1	22570.04272	0.00075
2	1	10	2	1	2	1	-1	10	1	0	1	22658.90179	0.00075
2	1	10	2	1	1	1	-1	10	1	0	1	22691.74864	0.00075
2	-1	10	2	1	1	1	1	10	1	0	1	22958.0652	0.00075
2	-1	10	2	1	2	1	1	10	1	0	1	23143.18458	0.00075
2	-1	10	2	1	1	1	1	10	1	1	2	25687.06011	0.00075
2	-1	10	2	1	2	1	1	10	1	1	2	25872.17892	0.00075
2	-1	10	2	1	1	1	1	10	1	1	1	25879.2673	0.00075
2	-1	10	2	1	2	1	1	10	1	1	1	26064.38734	0.00075

FTMW Transitions of PbF													
N'	P'	v'	J'	F'_1	F'	N''	P''	v''	J''	F''_1	F''	Measured Freq (MHz).	Unc.
2	1	11	2	1	2	1	-1	11	1	1	2	14329.36983	0.00075
2	1	11	2	2	3	1	-1	11	1	1	2	18199.42792	0.00075
2	1	11	2	2	2	1	-1	11	1	1	1	18246.41423	0.00075
2	-1	11	2	2	3	1	1	11	1	1	2	22416.68639	0.00075
2	-1	11	2	2	2	1	1	11	1	1	1	22444.02685	0.00075
2	1	11	2	1	2	1	-1	11	1	0	1	22556.93031	0.001
2	-1	11	2	1	2	1	1	11	1	0	1	23009.8026	0.001
2	1	12	2	1	2	1	-1	12	1	1	2	14197.29144	0.00075
2	1	12	2	2	3	1	-1	12	1	1	2	18066.08815	0.00075
2	1	12	2	2	2	1	-1	12	1	1	1	18112.69634	0.00075
2	-1	12	2	2	3	1	1	12	1	1	2	22291.81377	0.00075
2	-1	12	2	2	2	1	1	12	1	1	1	22318.36426	0.00075
2	1	13	2	2	3	1	-1	13	1	1	2	17933.48208	0.002
2	1	13	2	2	2	1	-1	13	1	1	1	17979.72033	0.00075
2	-1	13	2	2	3	1	1	13	1	1	2	22167.29671	0.00075
2	-1	13	2	2	2	1	1	13	1	1	1	22193.05379	0.00075
2	1	14	2	2	3	1	-1	14	1	1	2	17801.61828	0.002
2	1	14	2	2	2	1	-1	14	1	1	1	17847.48916	0.001
2	1	11	2	1	1	1	-1	11	1	0	1	22590.58422	0.001
2	1	15	2	2	3	1	-1	15	1	1	2	17670.49357	0.001
1	1	20	1	0	0	1	-1	20	1	1	1	3925.89105	0.0015
1	1	20	1	1	1	1	-1	20	1	0	0	4198.15822	0.0015
1	1	20	1	1	1	1	-1	20	1	1	1	4233.0993	0.0007
2	-1	20	2	1	1	2	1	20	2	1	1	8124.06457	0.001
2	-1	20	2	1	1	2	1	20	2	2	2	8206.61122	0.003
2	-1	20	2	2	2	2	1	20	2	1	1	8314.28438	0.0007
2	-1	20	2	2	2	2	1	20	2	2	2	8396.83017	0.001
2	1	20	2	2	2	1	-1	20	1	1	1	18429.54268	0.0005

FTMW Transitions of PbF													
N'	P'	v'	J'	F'_1	F'	N''	P''	v''	J''	F''_1	F''	Measured Freq (MHz).	Unc.
2	1	20	2	1	1	1	-1	20	1	0	0	18477.14786	0.0005
2	1	20	2	1	1	1	-1	20	1	1	1	18512.09022	0.0005
2	-1	20	2	2	2	1	1	20	1	1	1	22593.27178	0.0005
2	-1	20	2	1	1	1	1	20	1	0	0	22710.26738	0.0005
2	-1	20	2	1	1	1	1	20	1	1	1	22403.054	0.0005
2	1	21	2	2	2	1	-1	21	1	1	1	18295.15526	0.0005
2	1	21	2	1	1	1	-1	21	1	0	0	18341.90629	0.0005
2	1	21	2	1	1	1	-1	21	1	1	1	18379.09649	0.0015
2	-1	21	2	1	1	1	1	21	1	1	1	22270.00064	0.0005
2	-1	21	2	2	2	1	1	21	1	1	1	22460.82147	0.0005
2	-1	21	2	1	1	1	1	21	1	0	0	22577.472	0.0005
2	1	22	2	2	2	1	-1	22	1	1	1	18161.49498	0.0005
2	1	22	2	1	1	1	-1	22	1	0	0	18207.40547	0.001
2	1	22	2	1	1	1	-1	22	1	1	1	18246.8037	0.001
2	-1	22	2	1	1	1	1	22	1	1	1	22137.21082	0.001
2	1	23	2	2	2	1	-1	23	1	1	1	18028.56596	0.0005
2	1	23	2	1	1	1	-1	23	1	0	0	18073.65005	0.0005
2	1	24	2	2	2	1	-1	24	1	1	1	17896.3704	0.0005
2	1	25	2	2	2	1	-1	25	1	1	1	17764.91321	0.0005
2	-1	30	2	2	2	2	1	30	2	2	2	8403.7241	0.0006
2	1	30	2	2	2	1	-1	30	1	1	1	18444.7873	0.0005
2	1	30	2	1	1	1	-1	30	1	0	0	18492.39223	0.0005
2	1	30	2	1	1	1	-1	30	1	1	1	18527.33549	0.0005
2	-1	30	2	1	1	1	1	30	1	1	1	22421.74365	0.0005
2	-1	30	2	2	2	1	1	30	1	1	1	22611.96289	0.0005
2	-1	30	2	1	1	1	1	30	1	0	0	22728.95686	0.0005

End of Table